Taylor & Francis
Taylor & Francis Group

Combustion Science and Technology

ISSN: (Print) (Online) Journal homepage: www.tandfonline.com/journals/gcst20

# Modelling of the Flame Surface Density Transport During Flame-Wall Interaction of Premixed Flames within Turbulent Boundary Layers

Sanjeev Kumar Ghai, Umair Ahmed & Nilanjan Chakraborty

**To cite this article:** Sanjeev Kumar Ghai, Umair Ahmed & Nilanjan Chakraborty (10 Mar 2024): Modelling of the Flame Surface Density Transport During Flame-Wall Interaction of Premixed Flames within Turbulent Boundary Layers, Combustion Science and Technology, DOI: 10.1080/00102202.2024.2326649

**To link to this article:** https://doi.org/10.1080/00102202.2024.2326649



Published online: 10 Mar 2024.

COMBUSTION SCIENCE AND TECHNOLOGY
https://doi.org/10.1080/00102202.2024.2326649

Taylor & Francis
Taylor & Francis Group



# Modelling of the Flame Surface Density Transport During Flame-Wall Interaction of Premixed Flames within Turbulent Boundary Layers

Sanjeev Kumar Ghai, Umair Ahmed, and Nilanjan Chakraborty

School of Engineering, Newcastle University, Newcastle Upon Tyne, UK

**ABSTRACT**

A priori Direct Numerical Simulation (DNS) analysis of the modelling of the generalised flame surface density (FSD) transport equation in the framework of Reynolds Averaged Navier-Stokes (RANS) simulations has been conducted with a focus on flame-wall interaction (FWI) within turbulent boundary layers. The analysis was performed using two different scenarios: one involving the unsteady head-on interaction of a statistically planar premixed flame as it propagates through a turbulent boundary layer, and the other addressing statistically stationary oblique-wall interaction of a V-shaped premixed flame within a turbulent channel flow. Flame-wall interaction has been observed to exert a significant influence on the statistical behavior of the terms in the FSD transport equation. Throughout all phases of flame-wall interaction in both configurations, the primary source and sink terms in the FSD transport equation are consistently associated with the tangential strain rate and curvature terms. The relative importance of the contributions of the propagation and turbulent transport terms in the FSD transport equation have been found to be influenced by the flame-wall interaction configuration. Existing models for the tangential strain rate term in the FSD transport equation have been identified as inadequate based on a priori DNS assessment. Hence, adjustments to these models have been proposed to address the impact of flame orientation and near-wall effects specifically in the context of flame-wall interaction within turbulent boundary layers. The alignment between the flame normal vector and the wall normal vector has been identified as a crucial factor in modelling the contributions of unresolved dilatation rate and unresolved normal strain rate to the FSD transport equation. New models for these terms have been demonstrated to exhibit satisfactory agreement with the corresponding terms extracted from DNS data.

**ARTICLE HISTORY**
Received 22 December 2023
Revised 16 February 2024
Accepted 29 February 2024

**KEYWORDS**
Direct numerical simulations; oblique wall interaction; flame surface density; flame wall interaction; head on interaction

## Introduction

The analysis of flame-wall interaction (FWI) is vital for the advancement of modern combustion technologies. Modern combustion systems are designed to increase combustion efficiency, reduce emissions, and minimise energy consumption. However, modern combustion systems are made smaller in size in comparison to their earlier versions, aiming to enhance energy density. Moreover, these combustion systems are more susceptible to

**CONTACT** Sanjeev Kumar Ghai Sanjeev.ghai@newcastle.ac.uk School of Engineering, Newcastle University, Newcastle Upon Tyne, NE1 7RU, UK

flame quenching due to the heat transfer through the wall, a consequence of the high surface-to-volume ratio. Furthermore, the heat transfer rate at the combustor wall is pivotal for the design of cooling systems and determining optimum conditions to avoid thermal fatigue of combustor walls. However, the prediction of heat transfer rate and its optimisation depends on accurate predictions of burning and heat release rates. Modelling the mean or filtered value of the reaction rate poses a challenge in the context of Reynolds Averaged Navier-Stokes (RANS) and Large Eddy Simulations (LES) due to the highly non-linear nature of the chemical reaction rate, which is dependent on temperature and species concentrations. Within the framework of flamelet assumption-based turbulent premixed combustion modelling, the mean chemical reaction rate is usually expressed in terms of Flame Surface Density (FSD). The FSD serves as a measure of the flame surface area per unit volume (Candel and Poinsot 1990), and the rate of reactant consumption per unit area is estimated using data from laminar flames. The FSD can be modeled either through a straightforward algebraic expression (Abu-Orf and Cant 2000; Ahmed, Chakraborty, and Klein 2021a; Boger et al. 1998; Bray 1990; Cant and Bray 1989a, 1989b; Chakraborty and Klein 2008; Charlette, Meneveau, and Veynante 2002; Fureby 2005; Keppeler et al. 2014; Klein, Chakraborty, and Pfitzner 2016; Knikker, Veynante, and Meneveau 2002; Ma et al. 2013; Rasool, Klein, and Chakraborty 2022) incorporated into the transport equation of the Favre-averaged reaction progress variable or by solving the transport equation (Berger, Attili, and Pitsch 2022; Bruneaux et al. 1996; Bruneaux, Poinsot, and Ferziger 1997; Candel et al. 1990; Cant, Pope, and Bray 1991; Chakraborty and Cant 2007, 2009a, 2011, 2013; Duclos, Veynante, and Poinsot 1993; Han and Huh 2008; Hawkes and Cant 2000, 2001; Hernández-Pérez et al. 2011; Katragadda, Gao, and Chakraborty 2014; Katragadda, Malkeson, and Chakraborty 2011, 2014; Keil, Chakraborty, and Klein 2020; Luca et al. 2019; Ma et al. 2014; Papapostolou et al. 2019; Reddy and Abraham 2012; Sellmann et al. 2017; Trouvé and Poinsot 1994; Varma, Ahmed, and Chakraborty 2021, 2023; Veynante et al. 1996) for FSD in conjunction with the other conservation equations within the framework of Reynolds Averaged Navier-Stokes (RANS) or Large Eddy Simulation (LES) approaches. The algebraic closure of FSD is suitable when there is a balance between the generation and destruction rates of the flame surface area. However, a modeled transport equation may need to be solved when this equilibrium is disrupted, such as in the case of combustion instabilities.

The predominant share of existing analyses, which specifically address the statistical behavior and modelling of FSD are conducted in scenarios without walls. A limited number of studies (Ahmed et al. 2020; Alshaalan and Rutland 1998; Bruneaux, Poinsot, and Ferziger 1997; Sellmann et al. 2017) have focussed on the FSD modelling within the context of FWI and considered closures of FSD (Ahmed, Chakraborty, and Klein 2021a; Alshaalan and Rutland 1998; Bruneaux, Poinsot, and Ferziger 1997; Lai et al. 2022; Lai, Klein, and Chakraborty 2018; Sellmann et al. 2017) and FSD based mean chemical reaction rate closure within the framework of RANS for wall-bounded flows, utilising Direct Numerical Simulation (DNS) data. The findings of these analyses revealed that the influence of walls necessitates the incorporation of correction factors to address flame quenching resulting from wall heat loss. Jainski et al. (2017) have used experimental data for side wall quenching to demonstrate that an FSD algebraic model proposed earlier in a simple chemistry based analysis (Watkins, Li, and Cant 1996) provides consistent results with experimental measurements. A priori DNS analysis by Lai, Klein, and Chakraborty (2017) led to

modifications to the LES algebraic closures of FSD proposed by Fureby (2005) and Keppeler et al. (2014). Bruneaux, Poinsot, and Ferziger (1997) introduced modifications to the models of the unclosed terms in the FSD transport equation within the context of RANS. Their modifications aimed to consider FWI in a turbulent channel flow configuration. However, it is important to note that the analysis by Bruneaux, Poinsot, and Ferziger (1997) did not account for the effects of density change. Sellmann et al. (2017) in a recent study, utilised variable density DNS data for head-on interaction (HOI) of statistically planar flames in a canonical configuration. The objective of the analysis by Sellmann et al. (2017) was to extend the closures proposed in the literature for the unclosed terms of the FSD transport equation within the context of RANS. Gupta et al. (2022) employed FSD based LES modelling to study CO production in the near-wall region. The approach by Gupta et al. (2022) involved a priori analysis of DNS data for the HOI of turbulent premixed flames. Despite these efforts, the modelling of FSD transport in the context of RANS during FWI within variable density turbulent boundary layers remains unexplored in the existing literature. This gap is noteworthy, given that FWI commonly occurs within turbulent boundary layers in various engineering devices. The current study aims to fill this literature gap by examining three-dimensional DNS data for two distinct configurations. The first configuration involves the unsteady HOI of a statistical planar flame propagating into a turbulent boundary layer. The second configuration pertains to a statistically stationary scenario, specifically the oblique-wall Interaction (OWI) of a V-shaped premixed flame in a turbulent channel flow interacting with inert isothermal channel walls. Consequently, the primary objectives of this study are as follows:

(1) To examine the statistical behavior of the unclosed terms in the FSD transport equation in the presence of FWI.
(2) To assess the predictive abilities of existing closure models within the framework of RANS and, where required, to modify or propose new closures for the unclosed terms in the FSD transport equation. The goal is to account for near-wall behavior in the modelling of unclosed terms in the FSD transport equation so that it can be applied for the analysis of FWI within turbulent boundary layers.

The structure of the paper is as follows: Section 2 offers the mathematical background, while Section 3 briefly outlines the numerical implementation. In Section 4, the results are presented and discussed. The final section of the paper summarises the main findings and draws conclusions.

## Mathematical background

In the framework of premixed turbulent combustion, the scalar field is commonly described by a reaction progress variable, denoted as $c$. This quantity can be defined in a manner that ensures a monotonic increase from zero in the unburned gas mixture to one in the fully burned gas mixture, as follows:

$$c = (Y_{Ru} - Y_R)/(Y_{Ru} - Y_{Rb}) \tag{1}$$

In this specific context of premixed turbulent combustion, the symbol $Y_R$ represents the relevant mass fraction of the reactant, chosen as the fuel for the current analysis. The

subscripts $u$ and $b$ denote the values in the unburned and burned gas mixtures, respectively. The transport equation governing the Favre-mean reaction progress variable is given as follows:

$$\frac{\partial(\bar{\rho}\tilde{c})}{\partial t}+\frac{\partial\left(\bar{\rho}\tilde{u}_j\tilde{c}\right)}{\partial x_j}=\frac{\partial}{\partial x_j}\overline{\left(\rho D\frac{\partial c}{\partial x_j}\right)}+\bar{\dot{\omega}}-\frac{\partial\left(\overline{\rho u_j''c''}\right)}{\partial x_j} \tag{2}$$

where $\rho$ denotes the density, $u_j$ represents the $j^{\text{th}}$ component of velocity, $D$ is the diffusivity of progress variable and $\dot{\omega}$ is the reaction rate associated with the progress variable. Here, $\bar{q},\tilde{q}=\overline{\rho q}/\bar{\rho}$ and $q''=q-\tilde{q}$ represent the Reynolds average, Favre mean and Favre fluctuation of the general quantity $q$, respectively. The terms on the right-hand side of Equation (2) are unclosed and require closure. The quantity $\overline{\rho u_j''c''}$ represents the turbulent scalar flux term, and the closure for this turbulent scalar flux is detailed elsewhere (Chakraborty and Cant 2009b; Veynante et al. 1997). The combined molecular diffusion and reaction rate term, comprising the first and second terms on the right-hand side of Equation (2), can be modeled as follows (Chakraborty and Cant 2011; Katragadda, Malkeson, and Chakraborty 2011):

$$\frac{\partial}{\partial x_j}\overline{\left(\rho D\frac{\partial c}{\partial x_j}\right)}+\bar{\dot{\omega}}=\overline{(\rho S_d)}_s\Sigma_{gen} \tag{3}$$

Here, the surface average of the general quantity $q$ is denoted as $\overline{(q)}_s=\overline{q|\ \ c|}/\overline{|\ \ c|}$ and $S_d=(Dc/Dt)|\ \ c|$ is the local displacement speed and $\Sigma_{gen}=\overline{|\ \ c|}$ is the generalised FSD (Boger et al. 1998). Within the framework of RANS, the transport equation governing the FSD is formulated as follows (Candel and Poinsot 1990; Pope 1988):

$$\begin{aligned}\frac{\partial\Sigma_{gen}}{\partial t}+\frac{\partial\left(\widetilde{u}_j\Sigma_{gen}\right)}{\partial x_j}&=\underbrace{-\partial\left\{\left[\overline{(u_i)}_s-\tilde{u}_i\right]\Sigma_{gen}\right\}/\partial x_i}_{T_1}\\&+\underbrace{\overline{\left((\delta_{ij}-N_iN_j)\partial u_i/\partial x_i\right)}_s\Sigma_{gen}}_{T_2}\ \ \underbrace{-\partial\left[\overline{(S_dN_i)}_s\Sigma_{gen}\right]/\partial x_i}_{T_3}\\&+\underbrace{\overline{(S_d\partial N_i/\partial x_i)}_s\Sigma_{gen}}_{T_4}\end{aligned} \tag{4}$$

where $\vec{N}=-\ \ c/|\ \ c|$ is the local flame normal vector. The four terms on the right-hand side of Equation (4) are identified as the turbulent transport term ($T_1$), tangential strain rate term ($T_2$), propagation term ($T_3$) and curvature term ($T_4$). The terms $T_1$, $T_2$, $T_3$ and $T_4$ are unclosed and therefore require modelling. Using the 3D DNS data of unsteady HOI of a statistical planar flame and OWI of a statistically stationary V-shaped flame in a turbulent channel flow subjected to isothermal wall boundary conditions, the statistical behaviour and modelling of all these unclosed terms will be analysed in Section 4 of this paper.

## Numerical implementation

The DNS data employed in the present analysis was produced using the widely recognised three-dimensional compressible DNS code SENGA+ (Jenkins and Cant 1999). In SENGA+, the conservation equations governing mass, momentum, energy, and chemical species are resolved in nondimensional form and a tenth-order central difference scheme is employed to compute spatial derivatives at internal grid points, while an accuracy-reducing approach is gradually applied toward the non-periodic boundaries, reaching a second-order accuracy. Time advancement is achieved through the use of a low-storage explicit third order Runge-Kutta scheme. In this investigation, a stoichiometric methane-air mixture is considered as the reactants, and the unburned reactants are preheated to 730K (i.e., $T_u = 730K$), leading to a heat release rate parameter $\tau = (T_{ad} - T_u)/T_u = 2.3$ where $T_{ad}$ is the adiabatic flame temperature. In this current study, a single-step Arrhenius-type irreversible chemical reaction is utilised to enhance computational efficiency. This choice is made due to the computational cost associated with 3D DNS simulations involving detailed chemical kinetics, which remain prohibitively expensive for turbulent premixed combustion, especially for turbulent boundary layer flows. In several previous DNS studies, a single-step chemistry approach is utilised to analyse premixed FWI (Ahmed, Chakraborty, and Klein 2021a, 2021c, 2021b, Ahmed et al. 2023; Alshaalan and Rutland 1998; Bruneaux et al. 1996; Bruneaux, Poinsot, and Ferziger 1997; Ghai et al. 2022, 2022, 2022; Ghai, Ahmed, and Chakraborty 2023a; Ghai et al. 2023; Lai, Moody, and Chakraborty 2017; Lai, Klein, and Chakraborty 2017; Lai, Wacks, and Chakraborty 2018; Poinsot, Haworth, and Bruneaux 1993; Sellmann et al. 2017; Zhao, Wang, and Chakraborty 2018). Furthermore, as indicated in earlier analyses (Lai et al. 2022; Lai, Klein, and Chakraborty 2018), statistics pertaining to wall heat flux, and minimum quenching distance obtained from simple chemistry DNS (Alshaalan and Rutland 1998, 2002; Lai and Chakraborty 2016; Zhao, Wang, and Chakraborty 2018) agree well with those achieved using detailed chemistry DNS (Lai et al. 2022; Lai, Klein, and Chakraborty 2018; Zhao et al. 2023). Moreover, mean chemical reaction rate closures in FWI using FSD, and Scalar Dissipation Rate (SDR) based on a single-step chemistry approach have been demonstrated to be valid for hydrocarbon-air premixed FWI DNS with detailed chemistry (Lai et al. 2022; Lai, Klein, and Chakraborty 2018). Recent experimental investigations have shown that the FWI model based on simple chemistry (Watkins, Li, and Cant 1996) yields satisfactory outcomes in FWI of hydrocarbon-air flames within turbulent boundary layers when compared to experimental data (Jainski et al. 2017, 2017, 2018). Hence, the representation of FWI in hydrocarbon-air flames within turbulent boundary layers using simple single-step chemistry can, at the very least, be considered qualitatively accurate. In the simulations, standard values are selected for Prandtl number $Pr$ and the ratio of specific heat $\gamma$ (i.e., $Pr = 0.7$ and $\gamma = 1.4$). A Lewis number, $Le$ of unity and a Zel'dovich number $\beta = T_{ac}(T_{ad} - T_u)/T_{ad}^2 = 6.0$ are considered for both cases in the present study.It was demonstrated elsewhere (Keil et al. 2021a, 2021b) that the present thermochemistry captures the correct qualitative behaviour of the reaction-diffusion imbalance for the reaction progress variable $c$ transport equation.

To specify the initial conditions for the reacting flow simulation of the unsteady HOI configuration and for the inlet and initial conditions for the statistically stationary OWI of a V-flame configuration, a non-reacting fully developed turbulent channel flow solution corresponding to $Re_\tau = \left(\rho_0 u_{\tau,NR} h\right)/\mu_0 = 110$ is used where a streamwise pressure gradient

(i.e., $-\partial p/\partial x = \rho u_{\tau,NR}^2/h$ where $p$ is the pressure) is applied to maintain the desired friction velocity $u_{\tau,NR} = \sqrt{|\tau_{w,NR}|/\rho}$ where $\rho_0$ is the unburned gas density, $\tau_{w,NR}$ is the wall shear stress, $\mu_0$ is the unburned gas viscosity, $h$ is the channel half height and the subscript $NR$ represents the non-reacting channel flow. Simulations are conducted for a bulk Reynolds number of $Re_b = (2\rho_0 u_b h)/\mu_0 = 3285$ and here, $u_b = (1/2h)\int_0^{2h} u dy$ is the bulk mean velocity. While acknowledging the moderate value of the friction Reynolds number $Re_\tau$, of 110, Ghai et al. (2022) demonstrated that wall-normal variations of enstrophy and the dissipation rate of turbulent kinetic energy, normalised in terms of wall units for non-reacting flows with $Re_\tau = 110$ agree well with computational results from (Gorski, Wallace, and Bernard 1994) at $Re_\tau = 145$ and experimental results of Balint, Vukoslavcevic, and Wallace (1990) at $Re_\tau = 890$. In the channel flow configuration, the longitudinal integral length scale $L_{11}$ remains approximately equal to $h$ and the root-mean-square velocity fluctuation scales with $u_{\tau,NR}$ for $Re_\tau = 110$ (Ahmed et al. 2021), which give rise to the Karlovitz number $Ka = (u'/S_L)^{3/2}(L_{11}/\delta_{th})^{-1/2}$ value of 0.36 and Damköhler number $Da = (L_{11}S_L)/(u'\delta_{th})$ value of 15.80, indicating turbulent premixed combustion occurs in a corrugated flamelet regime combustion (Peters 2000) away from the wall.

In Figure 1, the schematic diagram illustrates the simulation domain utilised for the HOI configuration. Within this setup, the turbulent boundary layer forms on top of a chemically inert wall, and the initial flow conditions are established by a non-reacting, fully developed turbulent channel flow solution. The size of the simulation domain is $L_x \times L_y \times L_z = 10.69h \times 1.33h \times 4h$, and it is discretised using a uniform Cartesian grid of $1920 \times 240 \times 720$. This leads to a maximum value of $y^+ = \rho_0 u_{\tau,NR} y/\mu_0 = 0.6$ for the grid points located adjacent to the wall, where $y$ represents the distance from the wall. Thus, the chosen grid resolution ensures approximately 2 grid points within $y^+ = 1$ and 17 grid points within $y^+ = 10$, consistent with the recommendations outlined by Gruber et al. (2010); Moser, Kim, and Mansour (1999). Additionally, this grid spacing guarantees the presence of at least eight grid points within the thermal flame thickness $\delta_{th} = (T_{ad} - T_u)/max|\ \ T|_L$ for $S_L/u_{\tau,NR} = 0.7$, where $S_L$ is the unstretched laminar burning velocity and $T$ is the dimensional temperature. The flame is representative of the

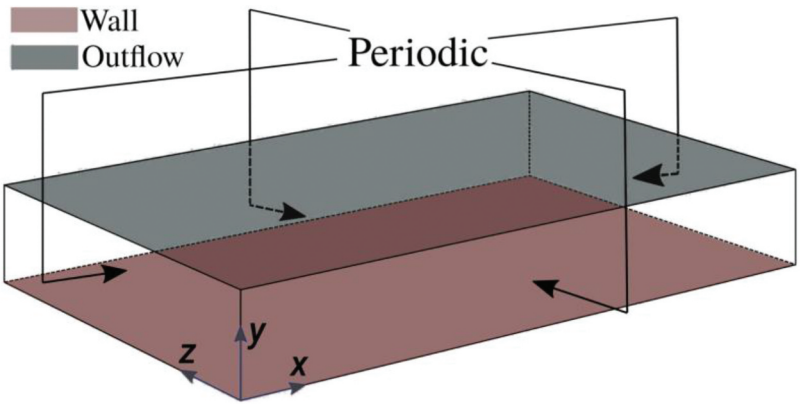


**Figure 1.** Diagram illustrating the simulation domain utilised for the unsteady HOI configuration.

corrugated flamelets regime combustion (Peters 2000) away from the wall in the current configuration which suggests that more than 8 grid points reside within the Kolmogorov length scale.

The domain boundaries in the streamwise (i.e., $x$) and spanwise (i.e., $z$) directions in Figure 1 are considered to be periodic. At $y = 0$, no-slip boundary condition is enforced, and the temperature of the unburned gas is specified (i.e., $T_w = T_u$) at the impenetrable inert wall. The boundary at $y/h = 1.33$ is treated as partially non-reflecting and the enhanced version of characteristic boundary conditions proposed by Yoo and Im (2007) has been employed. The 1-D steady state laminar flame solution has been interpolated to the 3-D simulation grid in such a way that the reactant side always faces the wall, whereas the outflow remains towards the product side in the $y-$direction. This initialisation also ensures that $c = 0.5$ based on the fuel mass fraction is obtained at close to $y/h \approx 0.85$. A streamwise constant mean pressure gradient is applied for the unsteady HOI case, similar to the approach used in non-reacting channel flow, to ensure the maintenance of a constant $Re_\tau$ throughout the simulation. The unsteady HOI simulation is continued for 2.0 flow through times, determined by the maximum streamwise axial mean velocity. This duration is equivalent to $21.30t_f$ where $t_f = \delta_{th}/S_L$ is the chemical timescale. Throughout this simulation period, the flame propagates and interacts with the wall. It is noteworthy that the turbulent boundary layer remains unchanged during this simulation time (Ahmed, Chakraborty, and Klein 2021b). For this simulation, the computation of one flow-through time took approximately 0.6 million CPU hours. In the unsteady HOI configuration, Reynolds and Favre-averaged quantities that account for correlations of Reynolds and Favre fluctuations are determined by spatially averaging the relevant quantities in the $x - z$ planes, which represent the periodic directions, at a specific time instance. Additional details about this configuration can be found in earlier publications (Ahmed, Chakraborty, and Klein 2021a, 2021b; Ghai et al. 2022).

Figure 2 illustrates the schematic diagram of the statistically stationary OWI of a turbulent V-flame within a channel. The dimensions of the simulation domain for the V-flame configuration is $L_x \times L_y \times L_z = 22.22h \times 2h \times 4h$, which is discretised by using a uniform Cartesian grid of $4000 \times 360 \times 720$ to ensure a minimum resolution of 0.6 in terms

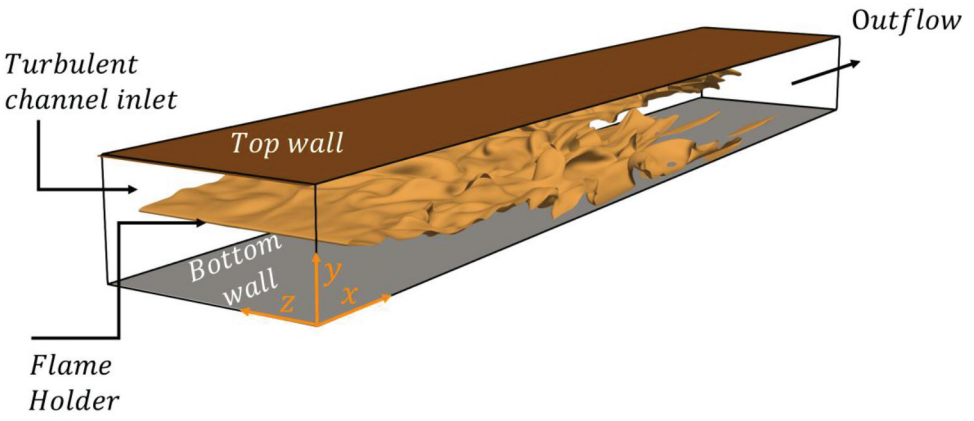


**Figure 2.** Schematic diagram for the statistically stationary turbulent V-flame OWI in a channel.

of $y^+$ and at least 8 grid points are situated within the flame thermal thickness $\delta_{th}$ (Ghai, Ahmed, and Chakraborty 2023b). More than 8 grid points are accommodated within the Kolmogorov scale away from the wall similar to the HOI case. The ratio of laminar flame speed to the friction velocity $S_L/u_{\tau,NR} = 0.7$ is considered for the present case. The flame holder with a radius of $0.2\delta_{th}$ is situated at the centre of the fully developed turbulent channel flow at $x/h = 0.83$ from the channel inlet. At the flame holder, the boundary conditions for velocity components and scalar variables are prescribed using the presumed Gaussian function (Dunstan et al. 2010) and additional information regarding the implementation of the flame holder is provided elsewhere (Ahmed, Chakraborty, and Klein 2021c) and not repeated here. The improved version of NSCBC is implemented to specify the boundary conditions (Yoo and Im 2007). The boundaries in the streamwise direction (i.e., $x$) are specified as turbulent inflow and partially non-reflecting outflow, respectively. The V-flame OWI simulation is conducted for isothermal boundary conditions (i.e., $T_w = T_u$) at $y = 0$ and $y = 2h$ with chemically inert and impenetrable walls. The spanwise boundaries (i.e., $z-$direction) are taken to be periodic. The simulation has been performed for 3.0 flow through times (1.0 flow through time to let the transient effects decay and subsequent 2.0 flow through times for sampling), based on the mean bulk velocity. The data from the last 2.0 flow through times has been utilised for post-processing. The Reynolds/Favre-mean values in the statistically stationary OWI setup are initially obtained by averaging in time and then averaging spatially in the periodic $(z)$direction. The symmetry about the centreline is exploited for averaging. The Reynolds/Favre-averaged quantities do not change significantly (at most by 1%) if only the half of the sampling duration is used for the averaging purpose. For this configuration, approximately 3.6 million CPU hours were needed for one flow-through time.

## Results and discussion

### *Interaction between the flame and the wall, and the statistical characteristics of FSD*

The isosurfaces of nondimensional temperature $\theta = 0.5$ (where $\theta = (T - T_u)/(T_{ad} - T_u)$) are shown in Figures 3a,b for turbulent boundary layer HOI at various normalised time instants $t/t_f$ (where $t_f = \delta_{th}/S_L$ is the chemical timescale) and for V-flame OWI configurations, respectively. The normalised distributions of vorticity magnitude $\Omega = \sqrt{w_i w_i} \times h/u_{\tau,NR}$ at $z/h = 2.0$ (where $w_i$ represents the $i^{th}$ component of vorticity) are shown in the background. The impact of vortical flow structures near the wall surface on the wrinkling of the flame surface is evident in Figures 3a,b. The flame undergoes quenching near the wall in both configurations investigated in this study as a result of heat loss through the cold isothermal wall surface. The flame starts to move and interact with the wall as time progresses in the case of HOI. The flame interacts with the wall for time instances $t/t_f \geq 10.92$ in the case of HOI. In contrast, the interaction between the flame and the wall initiates when $x/h \geq 12$ in the case of OWI.

The variations of the normalised generalised FSD $_{gen} \times \delta_Z = \overline{|\ c|} \times \delta_Z$ and the normalised resolved component of the FSD $|\ \bar{c}| \times \delta_Z$ (where $\delta_Z = \alpha_{T0}/S_L$ is the Zel'dovich flame thickness with $\alpha_{T0}$ being the unburned gas thermal diffusivity) with the normalised wall-normal distance $y/h$ are shown in Figure 4 for the unsteady HOI case at various normalised time instants $t/t_f$, and for the statistically stationary V-flame OWI case, at different

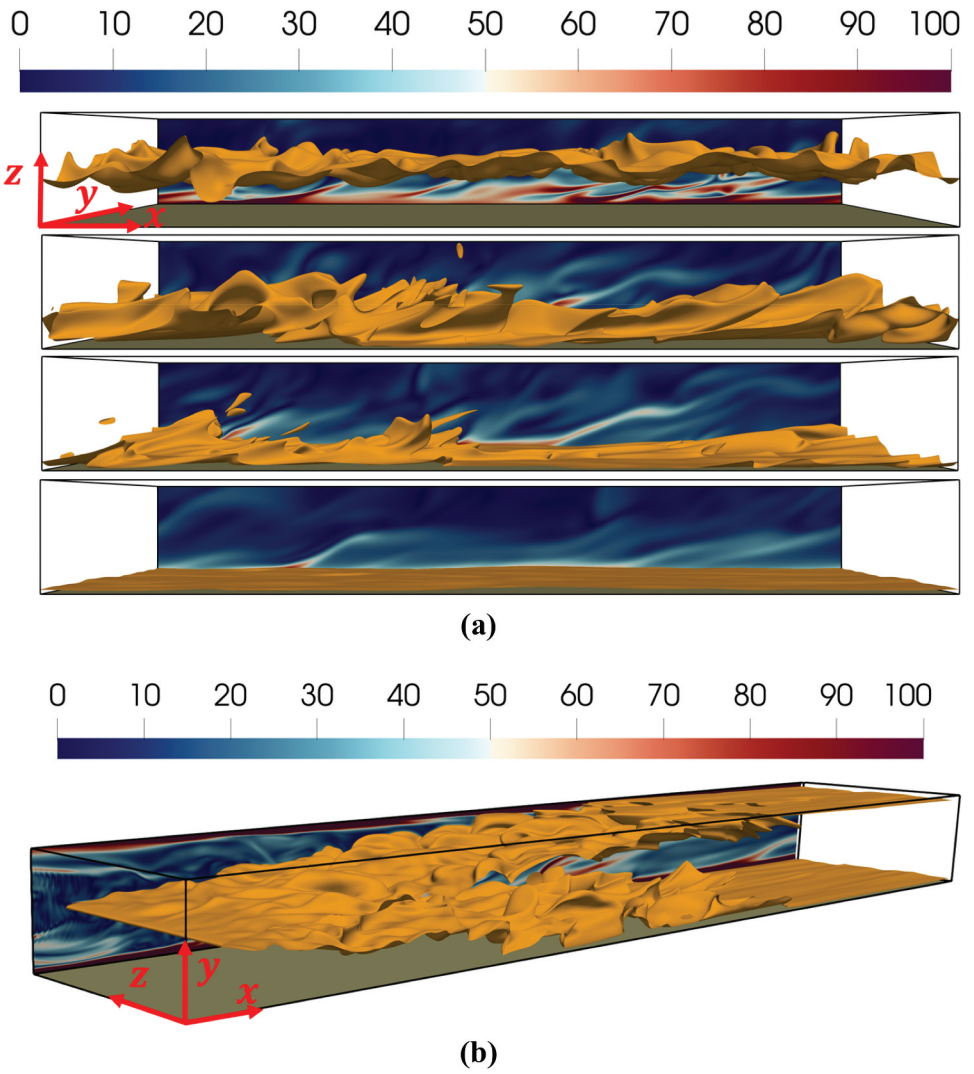


**Figure 3.** Isosurfaces of nondimensional temperature $\theta = 0.5$ for (a) unsteady HOI at various normalised time instants $t/t_f = 3.99, 10.92, 13.12$ and $16.27$ (top to bottom) and (b) statistically stationary V-flame OWI configurations. The normalised distributions of a vorticity magnitude $\Omega = \sqrt{w_i w_i} \times h/u_{\tau,NR}$ at $z/h = 2.0$ are shown in the background of the isosurfaces.

normalised streamwise distances $x/h$, respectively. As can be seen from Figure 4, the high values of $\Sigma_{gen}$ are noticeable in the proximity of the wall during the initial phases of FWI. However, $\Sigma_{gen}$ diminishes during the final stages of quenching when the boundary layer is predominantly filled with burned gas. The corresponding resolved part of the FSD $|\tilde{c}|$ also exhibits a qualitatively similar behaviour to that of generalised FSD $\Sigma_{gen}$. The extent of flame wrinkling can be quantified in terms of wrinkling factor $\Xi$, which can be defined as $\Xi = \Sigma_{gen}/|\tilde{c}|$. It can be observed from Figures 4c,d that $\Xi$ assumes greater values in the case of V-flame OWI as compared to the statistically planer HOI case during the initial stages of FWI when the flame is away from the wall. Figures 4c,d further indicate that $\Xi$

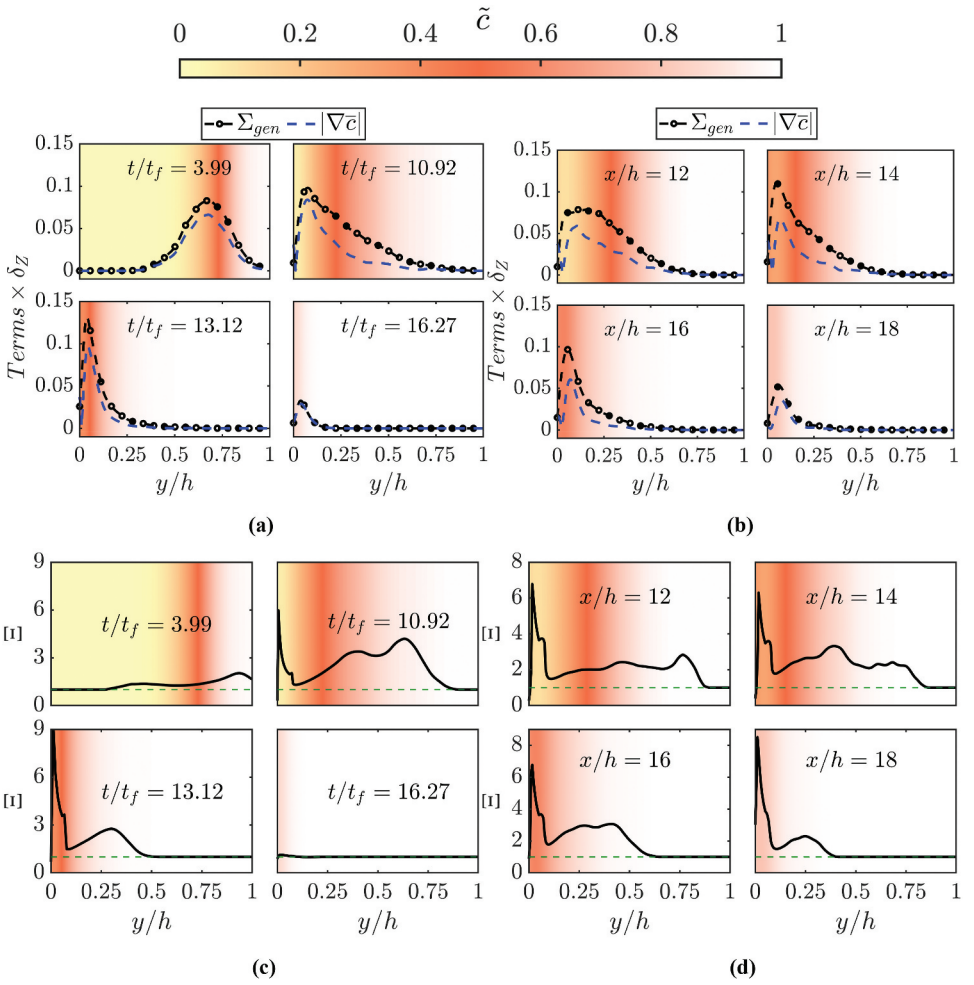


**Figure 4.** Variations of the normalised generalised FSD $_{gen} \times \delta_Z$ and normalised resolved FSD $|\bar{c}| \times \delta_Z$ with $y/h$ for the (a) unsteady HOI and (b) statistically stationary V-flame OWI. The wrinkling factor $\Xi$ with $y/h$ for the (c) unsteady HOI and (d) statistically stationary V-flame OWI. The wrinkling factor, $\Xi = 1$ is represented by green dashed line and the background color provides the local values of $\tilde{c}$.

diminishes near the wall, approaching 1.0 in the final stages of FWI for both configurations. This implies that the degree of flame wrinkling diminishes as flame quenching progresses. This behavior can be elucidated by examining the statistical characteristics of the terms in the FSD transport equation, as represented by Equation (4).

## *Statistical behaviour of the FSD transport equation*

The variations of the normalised unclosed terms of the FSD transport equation $\{T_1, T_2, T_3, T_4\} \times \delta_Z^2/S_L$ are shown in Figure 5 with the normalised wall-normal distance $y/h$ at various normalised time instants $t/t_f$ for the unsteady HOI case, and at different

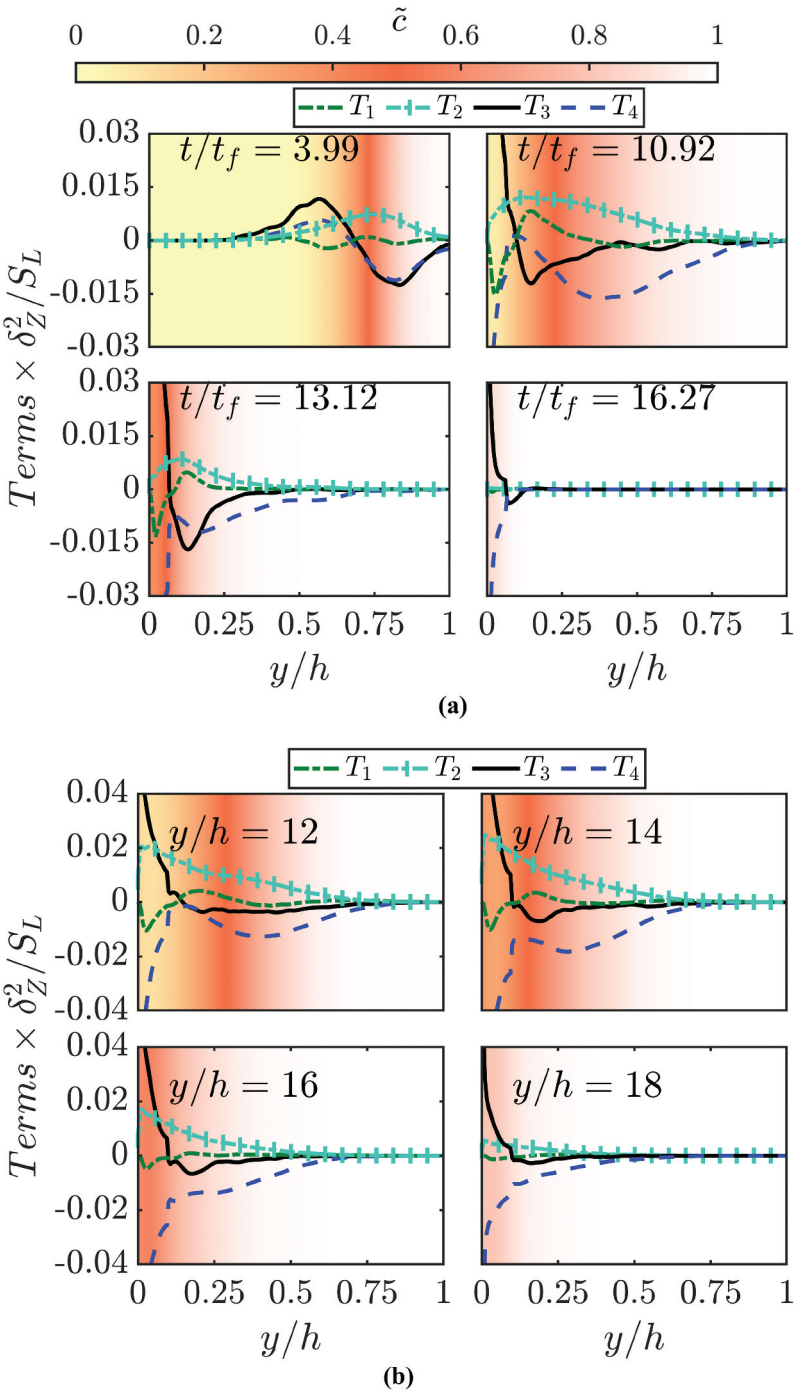


**Figure 5.** Variations of the $T_1, T_2, T_3$ and $T_4$ with $y/h$ for the (a) unsteady HOI and (b) statistically stationary V-flame OWI cases.

normalised streamwise distances $x/h$ for the statistically stationary V-flame OWI case. The findings from the results presented in Figure 5 reveal the following observations:

- The turbulent transport term $T_1$ remains positive when the flame is away from the wall in the burned region, and it becomes negative close to the wall during FWI for both configurations. The magnitude of the term $T_1$ progressively diminishes with the progress of flame quenching.
- The tangential strain rate term $T_2$ maintains a positive value across the entire domain, serving as a primary source term for both cases examined in this study.
- The propagation term $T_3$ exhibits positive values on the unburned side of the mixture and negative values on the burned side of the flame brush. Notably, during the advanced stages of flame quenching, $T_3$ assumes considerably large positive values near the wall.
- The curvature term $T_4$ exhibits mildly positive values in the unburned region and negative values in the burned region when the flame is at a distance from the wall. However, $T_4$ assumes large negative values near the wall as the flame interacts with the wall and starts to quench.

The behavior of the individual terms $\{T_1, T_2, T_3, T_4\}$ and their closures are explained in the subsequent sections of this paper.

## Modelling of the turbulent transport term $T_1$

The modelling of the turbulent transport term $T_1$ relies on the closure of the unclosed turbulent flux of FSD $\left[\overline{(u_i)}_s - \tilde{u}_i\right]\Sigma_{gen}$. In the HOI case, $\left[\overline{(u_2)}_s - \tilde{u}_2\right]\Sigma_{gen}$ is the only non-zero component of the FSD flux, whereas $\left[\overline{(u_1)}_s - \tilde{u}_1\right]\Sigma_{gen}$ and $\left[\overline{(u_2)}_s - \tilde{u}_2\right]\Sigma_{gen}$ are the non-zero components of the FSD flux in the OWI case. The normalised variations of the turbulent flux term $\left[\overline{(u_2)}_s - \tilde{u}_2\right]\Sigma_{gen} \times \delta_z/S_L$ with $y/h$ at different $t/t_f$ for the unsteady HOI case, and at different normalised streamwise distances $x/h$ for the V-flame OWI case are shown in Figure 6a,b, respectively. The variations of $\left[\overline{(u_1)}_s - \tilde{u}_1\right]\Sigma_{gen} \times \delta_z/S_L$ with $y/h$ at different normalised streamwise distances $x/h$ for the V-flame OWI case are shown in Figure 6c. As depicted in Figures 6a,b, the presence of the wall notably influences the turbulent flux of FSD $\left[\overline{(u_2)}_s - \tilde{u}_2\right]\Sigma_{gen}$, which displays positive values near the wall before diminishing once the flame undergoes quenching.

Usually, the turbulent flux of FSD $\left[\overline{(u_i)}_s - \tilde{u}_i\right]\Sigma_{gen}$ is modeled using a classical gradient hypothesis model (Cant, Pope, and Bray 1991; Hawkes and Cant 2000) in the following manner:

$$\left[\overline{(u_i)}_s - \tilde{u}_i\right]\Sigma_{gen} = -(\nu_t/Sc_t)\partial\Sigma_{gen}/\partial x_i \tag{5}$$

Here, $\nu_t$ and $Sc_t$ are the turbulent eddy viscosity and turbulent Schmidt number, respectively. The turbulent eddy viscosity $\nu_t$ can be calculated as follows:

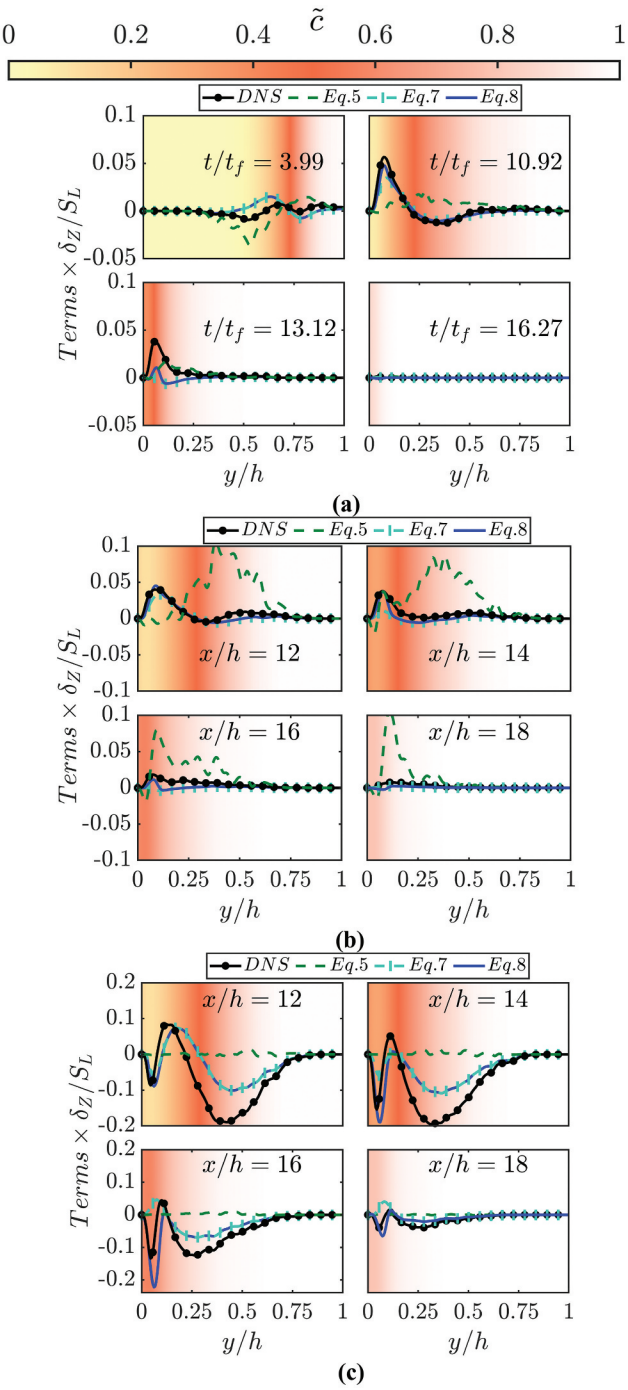


**Figure 6.** Variations of $\left[\overline{(u_2)}_s - \tilde{u}_2\right]\Sigma_{gen} \times \delta_Z/S_L$ with $y/h$ for the (a) unsteady HOI case at different times and (b) statistically stationary V-flame OWI case at different streamwise distances. (c) Variations of $\left[\overline{(u_1)}_s - \tilde{u}_1\right]\Sigma_{gen} \times \delta_Z/S_L$ with $y/h$ for the statistically stationary V-flame OWI case at different streamwise distances.

$$\nu_t = 0.09\tilde{k}^2/\tilde{\varepsilon} \tag{6}$$

Here $\tilde{k} = \overline{\rho u_i'' u_i''}/2\bar{\rho}$ and $\tilde{\varepsilon} = \overline{\mu\left(\partial u_i''/\partial x_j\right)\left(\partial u_i''/\partial x_j\right)}/\bar{\rho}$ are the kinetic energy and its dissipation rate, respectively.

The model predictions from Equation (5) are also shown in Figures 6a–c. It can be seen from Figures 6a–c that the predictions of Equation (5) do not capture the qualitative behavior of $\left[\overline{(u_i)}_s - \tilde{u}_i\right]\Sigma_{gen}$ and predict the opposite sign to the values obtained from DNS data. This is a consequence of $\left[\overline{(u_i)}_s - \tilde{u}_i\right]\Sigma_{gen}$ exhibiting a predominantly counter-gradient behaviour in the cases considered here. A counter-gradient behaviour is obtained when the flame normal acceleration as a result of thermal expansion overcomes the effects of turbulent flow fluctuations. The turbulent velocity fluctuations in the boundary layer can be scaled with respect to $u_{\tau,NR}$, whereas the velocity jump due to thermal expansion scales as $\tau S_L$. For the databases considered here $\tau S_L/u_{\tau,NR}$ remains greater than unity (i.e., $\tau S_L/u_{\tau,NR} = 1.61$) which suggests that the thermal expansion effects are expected to overwhelm the background turbulent fluctuations to yield counter-gradient transport for the cases considered here. It was demonstrated elsewhere (Chakraborty and Cant 2009b, 2011; Veynante et al. 1997) that the FSD flux shows gradient/counter-gradient transport when the turbulent scalar flux $\overline{\rho u_i'' c''}$ exhibits gradient/counter-gradient behaviour. Accordingly, a model for $\left[\overline{(u_i)}_s - \tilde{u}_i\right]\Sigma_{gen}$ was proposed which can predict both gradient and counter-gradient behaviours depending on the flow conditions in the following manner (Chakraborty and Cant 2009b, 2011):

$$\left[\overline{(u_i)}_s - \tilde{u}_i\right]\Sigma_{gen} = \frac{(A_2 - A_3\tilde{c})\overline{\rho u_i'' c''}\Sigma_{gen}}{\overline{\rho c''^2} + \bar{\rho}\tilde{c}(1-\tilde{c})} \tag{7}$$

where $A_2 = 1.0$ and $A_3 = 2$ are model parameters. Figures 6a–c reveal that Equation (7) captures the general behaviour of $\left[\overline{(u_i)}_s - \tilde{u}_i\right]\Sigma_{gen}$, but it consistently underestimates the magnitude of the turbulent flux term in the proximity of the wall. Nevertheless, the model predictions agree well with the DNS data when the flame is sufficiently away from the wall (Sellmann et al. 2017). It is perhaps not surprising because Equation (7) was proposed for flows without any FWI. Therefore, Sellmann et al. (2017) modified the parameters for unsteady HOI of statistically planar flames in canonical configuration to incorporate the near-wall effects. The modified expressions for $A_2$ and $A_3$ are given as (Sellmann et al. 2017):

$$A_2 = 1.06 - 0.06erf(y/\delta_Z - Pe_{min}) and A_3 = 0.93 + 1.07erf(y/\delta_Z - Pe_{min}) \tag{8}$$

where $Pe_{min} = y_Q/\delta_Z$ denotes the minimum Peclet number associated with the HOI of laminar premixed flames exhibiting identical thermochemistry, which is 2.14 for the present analysis. The model parameters $A_2$ and $A_3$ according to Equation (8) approaches 1.0 and 2.0, respectively when the flame is away from the wall (i.e., $y/\delta_Z \gg Pe_{min}$) and they increase and decrease respectively in the near wall region (i.e., $y/\delta_Z \ll Pe_{min}$). The model predictions obtained from Equation (7) with adjusted model parameters, as specified in Equation (8), exhibit a reasonably satisfactory agreement with the DNS data. This agreement is observed both away from the wall and in the near-wall region for the considered cases. However, there are some discrepancies in the quantitative prediction of Equation (8) and

DNS data, especially in the unsteady HOI case (e.g. underprediction near the wall at $t/t_f = 13.12$), but this model provides reasonable quantitative prediction in the statistically steady OWI case (see Figures 6b,c).

### Modelling of the tangential strain rate term $T_2$

The tangential strain rate term, $T_2$ can be decomposed into $T_D$, the contribution from the dilatation term and $T_N$, the contribution from the normal strain rate (Chakraborty and Cant 2011; Katragadda, Malkeson, and Chakraborty 2011; Sellmann et al. 2017),

$$T_2 = \underbrace{\overline{(\partial u_i/\partial x_i)_s}}_{T_D}{}_{gen} - \underbrace{\overline{\left(N_i N_j \partial u_i/\partial x_j\right)_s}}_{T_N}{}_{gen} \tag{9}$$

The dilatation term $T_D$ can be further partitioned into a resolved component $T_{D1}$ and an unresolved component $T_{D2}$ (Katragadda, Malkeson, and Chakraborty 2011; Sellmann et al. 2017; Varma, Ahmed, and Chakraborty 2021):

$$T_D = \underbrace{(\partial \tilde{u}_i/\partial x_i)|\ \bar{c}|}_{T_{D1}} + T_{D2} \tag{10}$$

The evaluation of $T_{D1}$ needs the knowledge of $\bar{c}$ but $\tilde{c}$ is available from RANS calculations. However, $\bar{c}$ can be determined from the $\tilde{c}$ as $\bar{c} = (1+\tau g^a)\tilde{c}/(1+\tau g^a \tilde{c})$ (Katragadda, Malkeson, and Chakraborty 2011; Sellmann et al. 2017; Varma, Ahmed, and Chakraborty 2021) where $a = 1.5$ is a model parameter and $g = \widetilde{c''^2}/[\tilde{c}(1-\tilde{c})]$ is the segregation factor. For $g = 1.0$, the bimodal distribution with peaks at $c = 0$ and $c = 1.0$ can be used to approximated the Probability density function (PDF) of $c$, and under this condition an exact relation given by $\bar{c} = (1+\tau)\tilde{c}/(1+\tau\tilde{c})$ can be obtained for unity Lewis number flames (Bray, Libby, and Moss 1985). Thus, the theoretical result relating $\bar{c}$ and $\tilde{c}$ can be recovered using $\bar{c} = (1+\tau g^a)\tilde{c}/(1+\tau g^a \tilde{c})$ for $g = 1.0$ but $\bar{c} = (1+\tau g^a)\tilde{c}/(1+\tau g^a \tilde{c})$ can be used to accurately extract $\bar{c}$ from $\tilde{c}$ when $g < 1$. It has been found that $\bar{c} = (1+\tau g^a)\tilde{c}/(1+\tau g^a \tilde{c})$ effectively predicts $\bar{c}$ under all conditions for both cases investigated in this study, which is not shown here for the sake of conciseness. Nonetheless, the comparison between $(\partial \tilde{u}_i/\partial x_i)|\ \bar{c}|$, derived from that $\bar{c} = (1+\tau g^a)\tilde{c}/(1+\tau g^a \tilde{c})$, and $T_{D1}$ extracted from DNS data is illustrated in Figure 7. This comparison indicates satisfactory agreement at all stages of FWI for both configurations utilised in this study.

For the unresolved part, $T_{D2} = \overline{(\partial u_i/\partial x_i|\ c|)} - (\partial \tilde{u}_i/\partial x_i)|\ \bar{c}|$ the following model expression for the term $T_{D2}$ has been proposed (Katragadda, Malkeson, and Chakraborty 2011; Sellmann et al. 2017; Varma, Ahmed, and Chakraborty 2021):

$$T_{D2} = (\tau S_L/\delta_{th})\left[A_4.(1-\tilde{c})^{\zeta}\left(\Sigma_{gen} - |\ \bar{c}|\right)\right]. \tag{11}$$

Here $A_4$ is the model parameter. Katragadda, Malkeson, and Chakraborty (2011) proposed $A_4 = 1.8/(1+Ka_L)^{0.35}$ (where $Ka_L = (\tilde{\varepsilon}\delta_{th})/S_L^{1.5}$ is the local Karlovitz number) and $\zeta = -0.3$ for the unity Lewis number flames based on a priori analysis of planar flames without FWI. The dependence of $A_4$ on the Karlovitz number ensures weakening of the influence of dilatation effects for large values of $Ka_L$. The model predictions are presented in Figure 8. For the unsteady HOI configuration, the model tends to overpredict $T_{D2}$ in the near-wall region. Conversely, in the statistically stationary OWI configuration, the model predictions exhibit reasonable

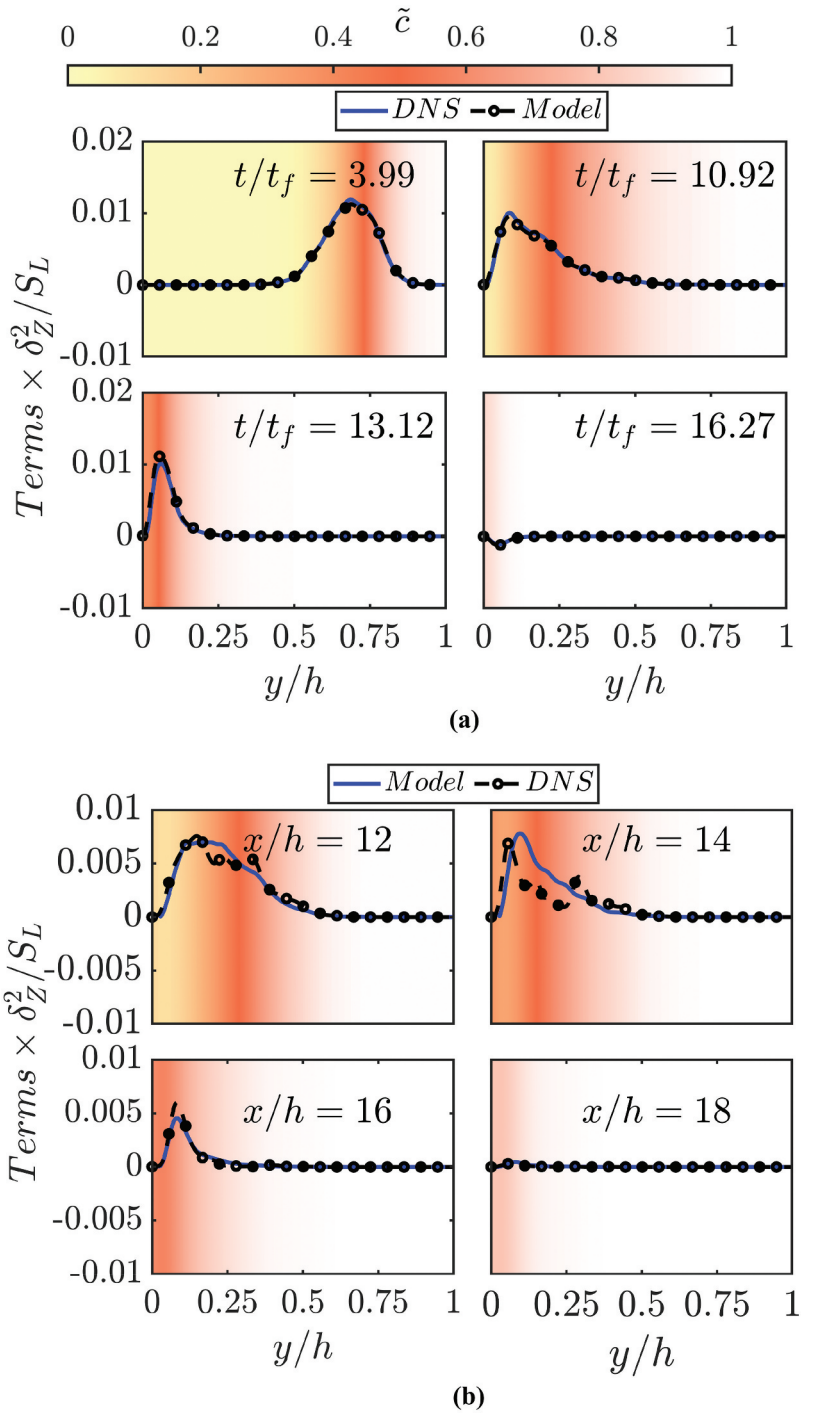


**Figure 7.** Variations of $T_{D1} \times \delta_Z^2/S_L$ with $y/h$ from DNS and model given by $\bar{c} = (1 + \tau g^a)\tilde{c}/(1 + \tau g^a \tilde{c})$ for the (a) unsteady HOI and (b) statistically stationary V-flame OWI cases. Figure 8

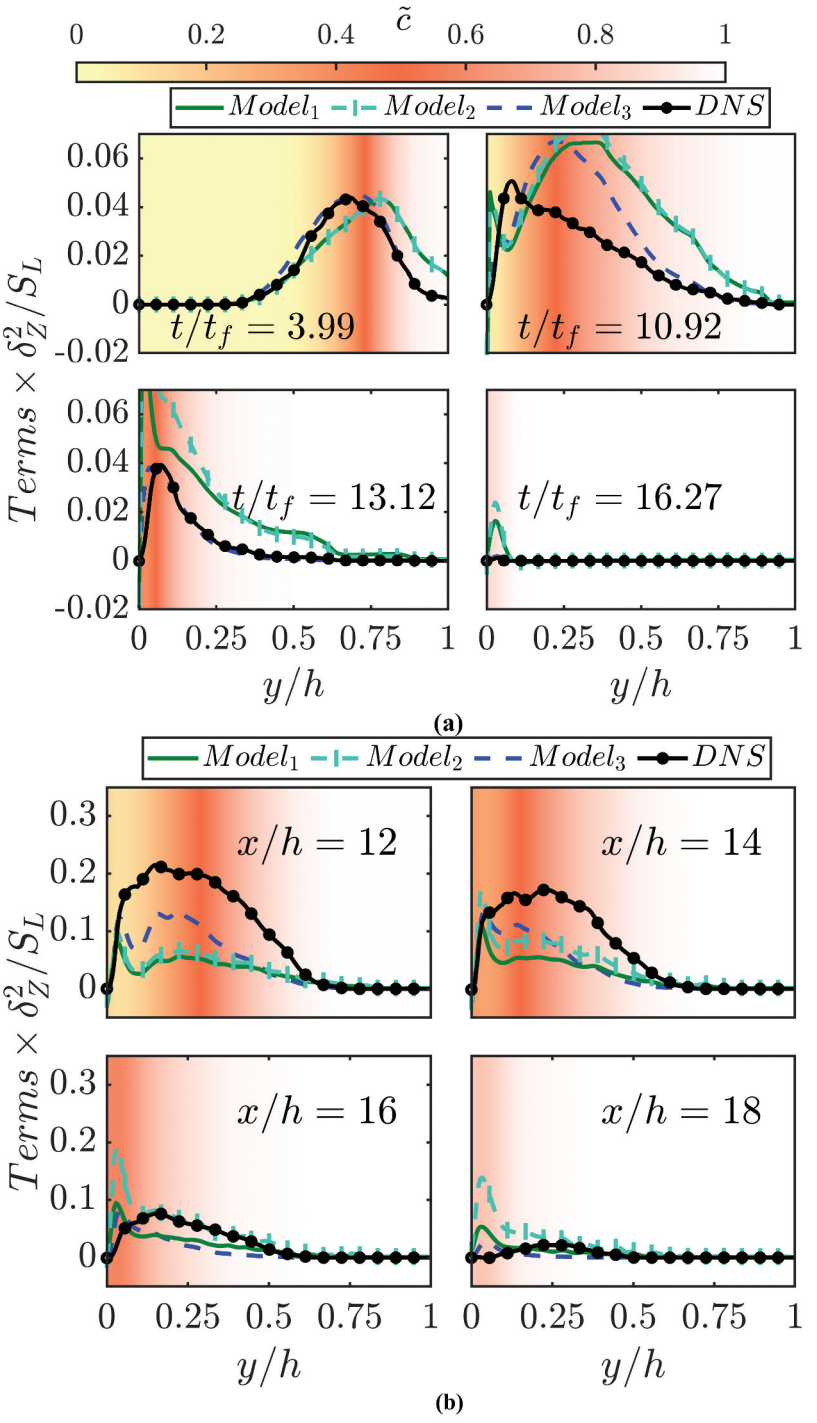


**Figure 8.** Variations of $T_{D2} \times \delta_Z^2/S_L$ with $y/h$ from DNS, model predictions given by Equation (11) with constants of ($Model_1$) Katragadda, Malkeson, and Chakraborty (2011) (green solid lines), with constants ($Model_2$) of Sellmann et al. (2017) (cyan dotted lines with symbols) and with $A_4$ and $\zeta$ ($Model_3$) given by Equation (12) (blue dashed lines) for the (a) unsteady HOI and (b) statistically stationary V-flame OWI cases.

agreement in the near-wall region but notably underpredict at all downstream locations. More recently, Sellmann et al. (2017) proposed $A_4 = 0.9exp\left(1.2\left(\tilde{c}_w - \tilde{\theta}_w\right)\right)(erf(y/\delta_Z) + 1)/(1 + Ka_L)^{0.35}\}$ and $\zeta = 1.5\exp\left[0.2\left(\tilde{c}_w - \tilde{\theta}_w\right)\right] - 1.8$ (where subscript w refers to the wall value) for the unsteady HOI without any fully developed boundary layer. Predictions with the model parameters suggested by Sellmann et al. (2017) are also shown in Figure 8. However, Equation (11) with $A_4$ and $\zeta$ suggested by Sellmann et al. (2017) inadequately capture the near-wall behaviour of $T_{D2}$ in the presence of shear within turbulent boundary layers, and the predictions remain almost comparable to the prediction of the earlier model suggested in (Katragadda, Malkeson, and Chakraborty 2011). In this analysis, the following parameterisations of $A_4$ and $\zeta$ have been proposed based on DNS data for both unsteady HOI and statistically stationary OWI configurations within turbulent boundary layers:

$$A_4 = 2.8[\mathrm{erf}(0.25y/\delta_Z) + 0.01] \times \left(1 + \left(\sqrt{\left(1 - \left(\vec{M}\cdot\vec{n}_w\right)^2\right)}\right)^{0.01}\right)/\left\{(1 + Ka_L)^{0.35}\right\} \text{ and } \zeta = 1.5\exp\left[0.2\left(\tilde{c}_w - \tilde{\theta}_w\right)\right] - 1.3 \tag{12}$$

In Equation (12), $\left(\tilde{c}_w - \tilde{\theta}_w\right)$ is an indicator of non-adiabaticity which acts as a quenching sensor, $\vec{M} = -\nabla\tilde{c}/|\nabla\tilde{c}|$ and $\vec{n}_w$ are the resolved flame normal vector and the wall normal vector, respectively. The parameter $\left(\tilde{c}_w - \tilde{\theta}_w\right)$ is active only near the wall during flame quenching and it reduces to zero away from the wall. The quantity $\vec{M}\cdot\vec{n}_w$ accounts for the orientation of the flame brush with respect to the wall. The error function and the orientation factor in the expression of $A_4$ ensure the correct magnitude of the term $T_{D2}$ in the proximity of the wall. It can be seen from Figure 8 that the predictions of Equation (11) with $A_4$ and $\zeta$ given by Equation (12) exhibit reasonable agreement both in the proximity to the wall and at a distance from it for both unsteady HOI and OWI configurations examined in this study. Nonetheless, there are slight underpredictions noted for the statistically stationary V-flame OWI case.

The contribution of the normal strain rate, denoted as $T_N$, can also be decomposed into two components: the resolved part, $T_{N1}$, and the unresolved part, $T_{N2}$ (Katragadda, Malkeson, and Chakraborty 2011; Sellmann et al. 2017; Varma, Ahmed, and Chakraborty 2021, 2023):

$$T_N = \underbrace{-\overline{(N_iN_j)}_s\left(\partial\widetilde{u}_i/\partial x_j\right)_{gen}}_{T_{N1}} \underbrace{-\overline{\left(N_iN_j\partial u_i^{''}/\partial x_j\right)}_{s\ gen}}_{T_{N2}} \tag{13}$$

The modelling of the resolved part $T_{N1}$ depends on the closure of $\overline{(N_iN_j)}_s$. Cant, Pope, and Bray (1991) proposed the following model considering the isotropic behaviour of the fluctuation contribution to $\overline{(N_iN_j)}_s$ in the following manner:

$$\overline{(N_iN_j)}_s = \overline{(N_i)}_s\overline{(N_j)}_s + (\delta_{ij}/3)\left[1 - \overline{(N_k)}_s\overline{(N_k)}_s\right] \tag{14}$$

Nonetheless, Veynante et al. (1996) experimentally established that flame normal fluctuations exhibit anisotropy and proposed the following model for $\overline{(N_iN_j)}_s$ as follows:

$$\overline{\left(N_i N_{j=i}\right)}_s = \sum_{k\neq i} \widetilde{u_k'' u_k''}/4\tilde{k} \text{ and } \overline{\left(N_i N_{j\neq i}\right)}_s = \widetilde{u_i'' u_j''}/2\tilde{k} \tag{15}$$

The predictions of $T_{N1}$ according to Equations (14) and (15) are compared with DNS data in Figure 9 for both unsteady HOI at various $t/t_f$ and for the statistically stationary V-flame OWI case at different $x/h$. It is evident from Figure 9 that both Equations (14) and (15) provide reasonably accurate predictions of $T_{N1}$ for both the cases examined in this study when the flame is sufficiently away from the wall. Notably, the predictions from Equation (14) agree more closely with the DNS data than those from Equation (15), primarily because the effects of anisotropy of flame normal fluctuations are less significant near the wall. Consequently, the model predictions according to Equation (14) consistently demonstrate the agreement with DNS data, both in the proximity of the wall and at a distance away from it.

In the previous studies (Katragadda, Malkeson, and Chakraborty 2011; Sellmann et al. 2017; Varma, Ahmed, and Chakraborty 2021, 2023), the fluctuating component of the normal strain rate contribution $T_{N2}$ modeled in the following manner.:

$$T_{N2} = \left(\tilde{\varepsilon}/\tilde{k}\right)[C_1 - \tau C_2 Da_L]\Sigma_{gen} \tag{16}$$

where $C_1$, $C_2$, are the model parameters and $Da_L = \tilde{k}S_L/(\tilde{\varepsilon}\delta_{th})$ is the local Damköhler number.

Equation (16) accounts for the alignment of $c$ with local principal strain rates (Katragadda, Malkeson, and Chakraborty 2011; Sellmann et al. 2017; Varma, Ahmed, and Chakraborty 2021, 2023). It has been demonstrated elsewhere (Chakraborty and Swaminathan 2007; Chakraborty, Klein, and Swaminathan 2009) that $c$ tends to align predominantly with the eigenvector linked to the most compressive principal strain rate when $\tau Da < 1$. This indicates that turbulent straining takes precedence over the strain rate induced by the flame normal acceleration. In contrast, when $\tau Da \gg 1$, a preferential alignment of $c$ with the eigenvector linked to the most extensive principal strain rate occurs. This alignment results from the dominance of strain rate induced by flame normal acceleration, surpassing the effects of turbulent straining (Chakraborty and Swaminathan 2007; Chakraborty, Klein, and Swaminathan 2009). It is possible to express $T_{N2}$ as (Katragadda, Malkeson, and Chakraborty 2011; Sellmann et al. 2017; Varma, Ahmed, and Chakraborty 2021, 2023):

$$T_{N2} = -\overline{\left(e_\alpha \cos^2\theta_\alpha + e_\beta \cos^2\theta_\beta + e_\gamma \cos^2\theta_\gamma\right)|\ c|} \tag{17}$$

Here $e_\alpha, e_\beta$ and $e_\gamma$ represents the most extensive, intermediate and the most compressive principal fluctuating strain rate tensor defined as $0.5\left(\partial u_i''/\partial x_j + \partial u_j''/\partial x_i\right)$. Additionally, $\theta_\alpha, \theta_\beta$ and $\theta_\gamma$ denotes the angles between $c$ and the eigenvectors associated with $e_\alpha, e_\beta$ and $e_\gamma$, respectively. Equation (17) suggests that a positive value of $T_{N2}$ is obtained when $c$ preferentially aligns with the eigenvector associated with $e_\gamma$ (i.e., $\cos^2\theta_\gamma = 1.0$). By contrast, a negative value of $T_{N2}$ is obtained when $c$ preferentially aligns with the eigenvector associated with $e_\alpha$ (i.e., $\cos^2\theta_\alpha = 1.0$). The model given by Equation (16) accounts for all the aforementioned alignment behaviours. In Equation (16), the term $C_1(\tilde{\varepsilon}/\tilde{k})\Sigma_{gen}$ accounts for the positive contribution of $T_{N2}$ (i.e., generation of the FSD) due to the preferential

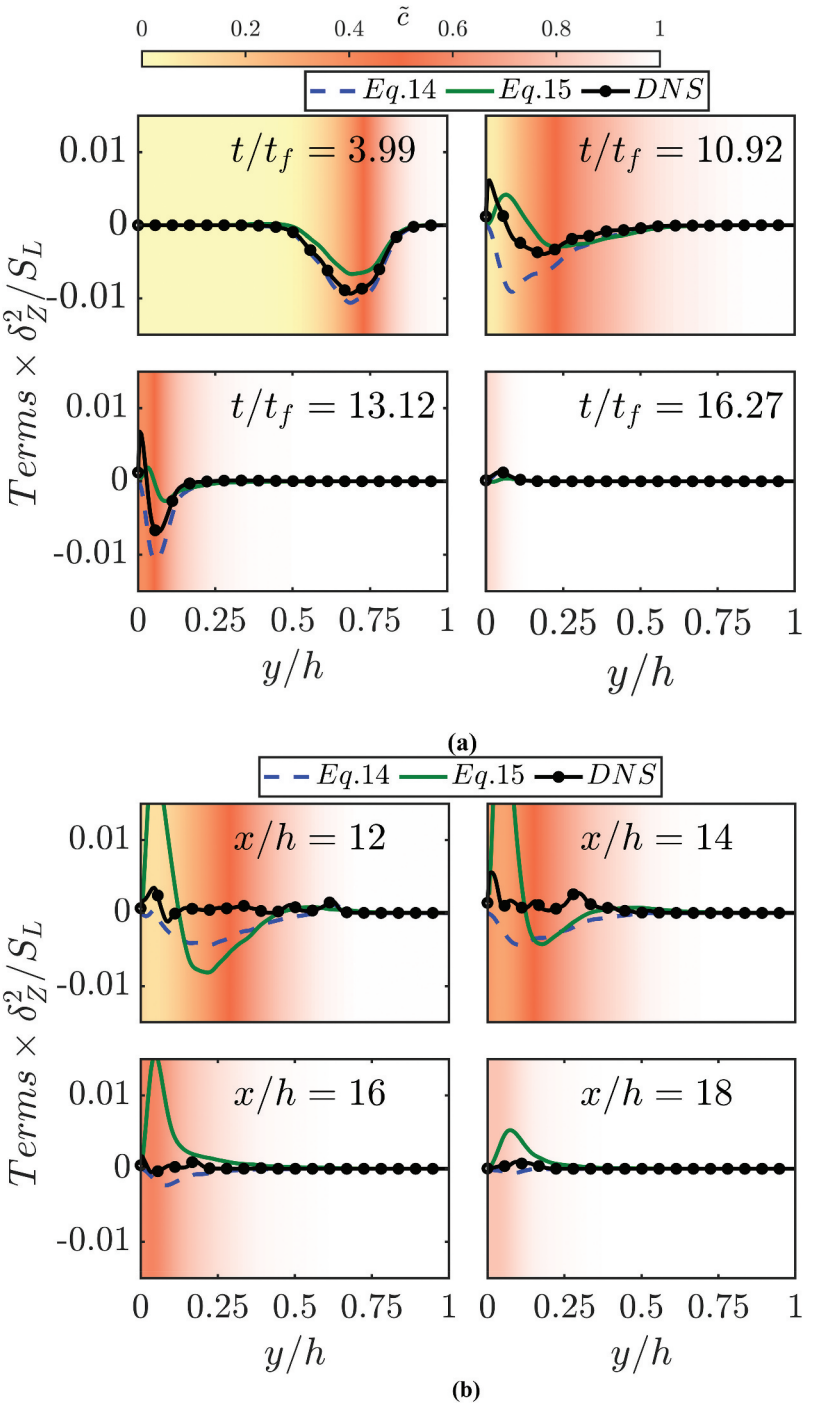


**Figure 9.** Variations of $T_{N1} \times \delta_Z^2/S_L$ with $y/h$ from DNS and with the $\overline{(N_i N_j)}_s$ models given by Equations (14) and (15) for the (a) unsteady HOI and (b) statistically stationary V-flame OWI cases.

alignment of $c$ with the eigenvector associated with $e_\gamma$ due to the dominance of the turbulent straining ($\sim\tilde{\varepsilon}/\tilde{k}$) over the heat release effects. By contrast, $-\left(\tilde{\varepsilon}/\tilde{k}\right)\tau C_2 Da_L \Sigma_{gen} = -\tau C_2 (S_L/\delta_{th})\Sigma_{gen}$ accounts for the negative contribution of $T_{N2}$ due to the preferential alignment of $c$ with the eigenvector associated with $e_\alpha$ as a result of the dominance of the strain rate induced by the flame normal acceleration ($\sim\tau S_L/\delta_{th}$) over turbulent straining. Sellmann et al. (2017) proposed $C_1 = \mathrm{erf}(0.1y/\delta_Z)$ and $C_2 = A_5\left(1 - \overline{(N_k)}_s\overline{(N_k)}_s\right)/(1 + Ka_L)^{0.35}$ derived from a previous a priori DNS analysis of unsteady HOI in a canonical configuration without a developed boundary layer, where $A_5$ was expressed as:

$$A_5 = 0.471\mathrm{erf}(0.5 \cdot x_1/\delta_Z)\exp\left(2\left(\tilde{c}_w - \tilde{\theta}_w\right)\right)\left[\frac{0.3}{\mathrm{erf}(Re_L + 0.01)^{0.5\exp(-\tilde{c}_w)}}\right]^{A_6} \tag{18}$$

In the above expression $A_6 = 0.5\left(\mathrm{erf}\left(-y/\delta_Z + Pe_{min}^3\right) + 1\right)$ and $Re_L = \rho_0\tilde{k}^2/\mu_0\tilde{\varepsilon}$ is the local turbulent Reynolds number with $\mu_0$ being the unburned gas viscosity. The predictions of the model given by Equation (16) according to $C_1$ and $C_2$ proposed by Sellmann et al. (2017) are compared to $T_{N2}$ extracted from DNS data in Figure 10 for unsteady HOI case at various $t/t_f$ and for the V-flame OWI case at different $x/h$. It can be seen from Figure 10 that Equation (16) with $C_1$ and $C_2$ proposed by Sellmann et al. (2017) does not adequately capture the behaviour of $T_{N2}$ for the cases considered here and the disagreement is particularly strong for the V-flame case. It is worth noting that the model parameters proposed by Sellmann et al. (2017) were not calibrated for turbulent boundary layer transport. The results obtained from Figure 10 seem to suggest that the relative orientation between $\vec{M}$ and $\vec{n}_w$ plays a key role in the performance of the model given by Equation (16). This is accounted for in this work by modifying $A_5$ in the following manner:

$$A_5 = 1.5\left[\mathrm{erf}(0.5.y/\delta_Z) + 0.01\right]\mathrm{erf}\left[0.5\left(\widetilde{c_w} - \widetilde{\theta_w}\right) + 1\right] \times \left(1 + \left(\sqrt{\left(1 - \left(\vec{M}\cdot\vec{n}_w\right)^2\right)}\right)^{0.01}\right) \tag{19}$$

In Equation (19), $[\mathrm{erf}(0.5.y/\delta_Z) + 0.01]$ allows for the gradual increase of $T_{N2}$ in the wall-normal distance. The correct magnitude of $T_{N2}$ in the near wall region has been captured by the combined actions of both error functions. The flame orientation has been accounted for by $\vec{M}\cdot\vec{n}_w$ and the factor $\left(\tilde{c}_w - \tilde{\theta}_w\right)$ acts as a quenching sensor which ensures that the magnitude of $T_{N2}$ is accurately captured during the flame quenching. It can be seen from Figure 10 that Equation (16) with $C_1 = \mathrm{erf}(0.1y/\delta_Z)$ and $C_2 = A_5\left(1 - \overline{(N_k)}_s\overline{(N_k)}_s\right)/(1 + Ka_L)^{0.35}$ (with $A_5$ given by Equation (19)) captures the variation of $T_{N2}$ both near the wall as well as away from the wall for both the configurations considered in the present analysis.

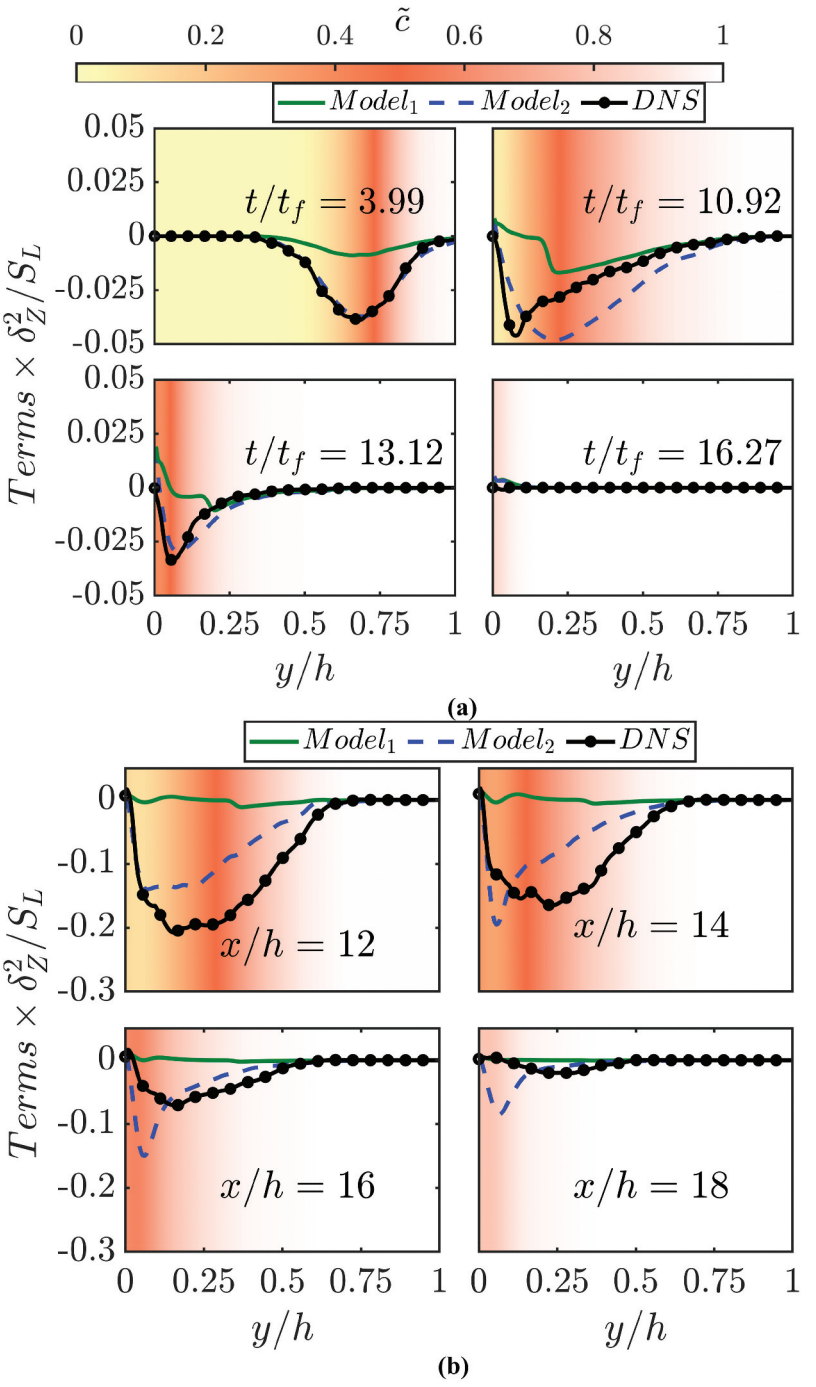


**Figure 10.** Variations of $T_{N2} \times \delta_Z^2/S_L$ with $y/h$ from DNS and model predictions from Equation (16) with $C_1$ and $C_2$ proposed by Sellmann et al. (2017) (Model 1) and Equation (16) with $C_1 = \mathrm{erf}(0.1y/\delta_Z)$ and $C_2 = A_5\left(1 - \overline{(N_k)}_s\overline{(N_k)}_s\right)/(1 + Ka_L)^{0.35}$ (with $A_5$ given by Equation (19)) (Model 2) for the (a) unsteady HOI and (b) statistically stationary V-flame OWI cases.

### *Modelling of the propagation and curvature terms* $(T_3 + T_4)$

The curvature and propagation terms in the context of FSD transport are often modeled together (Berger, Attili, and Pitsch 2022; Cant, Pope, and Bray 1991; Chakraborty and Cant 2011, 2013; Han and Huh 2008; Papapostolou et al. 2019; Sellmann et al. 2017; Trouvé and Poinsot 1994; Varma, Ahmed, and Chakraborty 2021, 2023). The variations of the combined curvature and propagation terms $(T_3 + T_4)$ in the wall-normal direction are shown in Figure 11 for the unsteady HOI case, at various $t/t_f$, and at different values of $x/h$ for the V-flame OWI case. It is evident from Figure 11 that the combined contribution of $(T_3 + T_4)$ assumes positive (negative) values towards the reactant (product) side of the flame brush. Qualitatively similar behaviour has been reported in various previous studies without the presence of the wall (Chakraborty and Cant 2011; Hawkes and Cant 2000; Katragadda, Malkeson, and Chakraborty 2011). In Figure 5, it is evident that the propagation term $T_3$ and the curvature term $T_4$ exhibit positive and negative values, respectively, in the vicinity of the wall. The values of $T_3$ and $T_4$ are almost equal in magnitude close to the wall in the unsteady HOI case, whereas for the statistically stationary V-flame OWI case, the contribution arises from the curvature term $T_4$, which is higher in magnitude than the propagation term $T_3$. Therefore, the combined contribution of $(T_3 + T_4)$ is negative even towards the unburned gas side of the flame brush for the V-flame OWI case. Bruneaux, Poinsot, and Ferziger (1997) introduced distinct models for the terms $T_3$ and $T_4$ (i.e., $T_3 = -\partial\left(S_L M_i \Sigma_{gen}\left(1-(1-Q_m)/\gamma_\omega\right)\right)/\partial x_i$and $T_4 = -S_L\Sigma_{\text{gen}}^2/\bar{c}(1-\bar{c})$ with $\gamma_\omega = 0.3$, $Q_m = \exp\left[-2\beta\left(\tilde{c}-\tilde{\theta}\right)\right]$) but Sellmann et al. (2017) showed that for the canonical HOI configuration that the models proposed by Bruneaux, Poinsot, and Ferziger (1997) do not capture the qualitative behaviour of the combined contribution $(T_3 + T_4)$ obtained from the DNS data. The cases examined here exhibit the same qualitative behaviour, and the combined predictions from the models proposed by Bruneaux, Poinsot, and Ferziger (1997) are illustrated in Figure 11. The model by Bruneaux, Poinsot, and Ferziger (1997) gives an incorrect estimation of the combined contribution $(T_3 + T_4)$ in the region close to the wall for both the configuration considered in this study. However, away from the wall the models by Bruneaux, Poinsot, and Ferziger (1997) reasonably capture the variation of the combined contribution of $(T_3 + T_4)$. The combined contribution of $T_3$ and $T_4$ is typically modeled as follows for premixed flames without any influence from walls (Chakraborty and Cant 2011, 2013; Han and Huh 2008; Katragadda, Gao, and Chakraborty 2014; Papapostolou et al. 2019; Sellmann et al. 2017; Varma, Ahmed, and Chakraborty 2021, 2023):

$$(T_3 + T_4) = -\frac{\partial}{\partial x_i}\left[\frac{\rho_0 S_L}{\bar{\rho}}\overline{(N_i)}_s\Sigma_{gen}\right] + \frac{\rho_0 S_L}{\bar{\rho}}\frac{\partial\overline{(N_i)}_s}{\partial x_i}\Sigma_{gen} - \beta_0\left[1-\overline{(N_k)}_s\overline{(N_k)}_s\right]\frac{\left(\bar{c}-c_{cp}\right)S_L\Sigma_{gen}^2}{\bar{c}(1-\bar{c})} \tag{20}$$

Here $\beta_o > 1.0$ (Duclos, Veynante, and Poinsot 1993) and $c_{cp}$ are the model parameters. The presence of the wall results in a significant reduction in the flame propagation rate during the process of flame quenching. To account for the reduction in the flame propagation rate, Sellmann et al. (2017) proposed a modification to Equation (20). In the modified expression, Sellmann et al. (2017) replaced the laminar flame speed $S_L$ with a modified expression

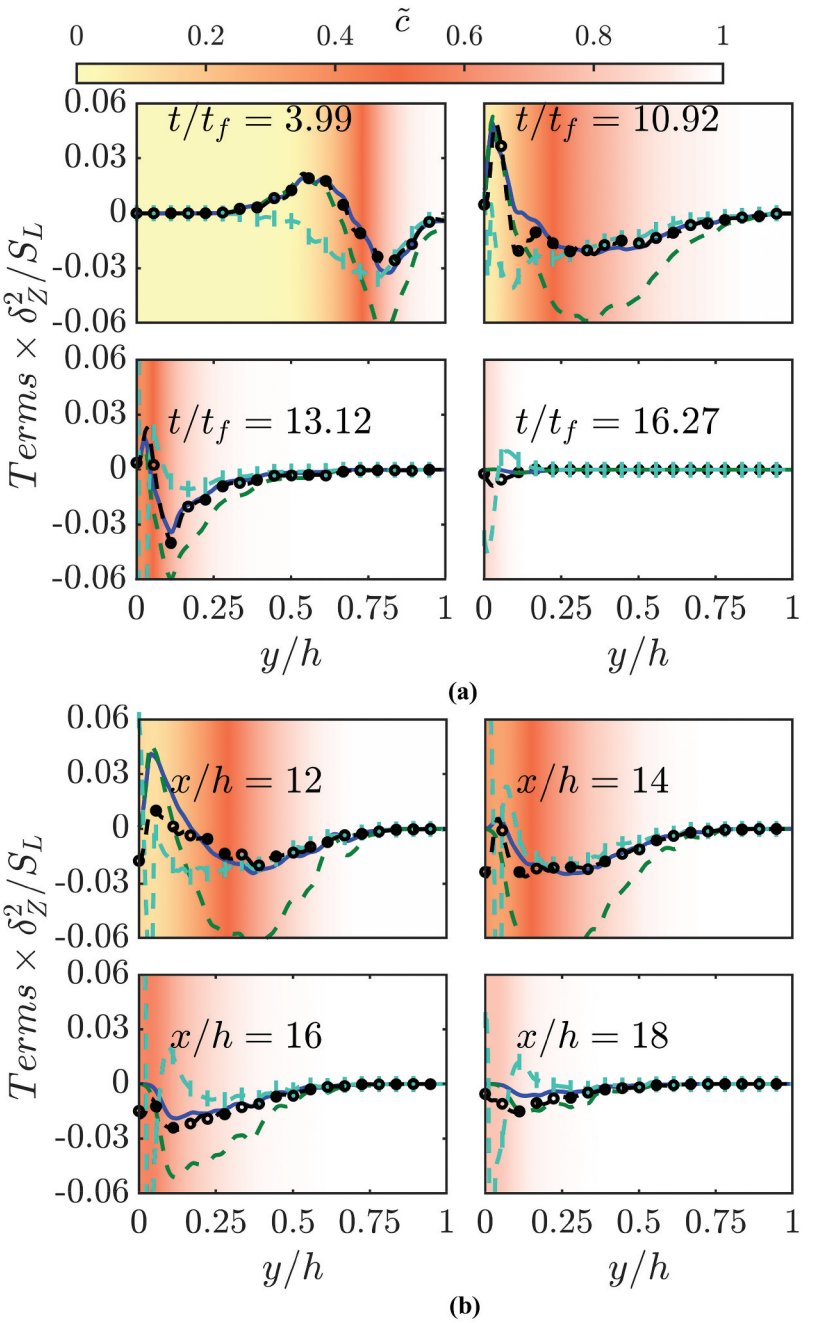


**Figure 11.** Variations of $(T_3 + T_4) \times \delta_Z^2/S_L$ with $y/h$ as obtained from DNS (black symbols), predictions of the model from Bruneaux, Poinsot, and Ferziger (1997) (cyan dashed symbol lines), predictions of Equation (20) (where $S_L$ is replaced by $S_L^{'}$) with $\beta_o = 8.0$ and $c_{cp} = 0.35$ (green broken line) and with $\beta_o = 4.0$ and $c_{cp} = 0.5$ (blue line) for the (a) unsteady HOI and (b) statistically stationary V-flame OWI cases.

for the flame speed $S_L^{'} = S_L \exp\left[-8.0\left(\tilde{c} - \tilde{\theta}\right)\right]$, and it can be seen from Figure 11 that Equation (20) for $\beta_o = 8.0$ and $c_{cp} = 0.35$ provides a satisfactory agreement with DNS data in the unburned region of the flame and also in the near wall region for the unsteady HOI configuration considered in the present work. It can also be seen from Figure 11 that Equation (20) with $\beta_o = 4.0$ and $c_{cp} = 0.5$ provide a satisfactory agreement with $(T_3 + T_4)$ obtained from DNS data when the flame remains away from the wall in both configurations. However, Equation (20) even with $S_L^{'} = S_L \exp\left[-8.0\left(\tilde{c} - \tilde{\theta}\right)\right]$ overpredicts the magnitude in the region close to the wall for the statistically stationary V-flame OWI case, which is not unexpected because Equation (20) was calibrated for flows in the absence of any mean shear and in the absence of walls. Hence, there is still potential for improvement in the modelling of $(T_3 + T_4)$ during FWI.

### *Closure for the mean chemical reaction rate* $\overline{\dot{\omega}}$

Figure 12 shows the variations of the normalised mean chemical reaction rate $\overline{\dot{\omega}} \times \delta_Z/\rho_0 S_L$ with the normalised wall-normal distance $y/h$ for the unsteady HOI case at various $t/t_f$, and the V-flame OWI case, at different values of $x/h$. In the context of RANS, the contribution from the mean molecular diffusion rate term, $\overline{\quad \cdot (\rho D \quad c)}$ is often considered negligible in comparison to the mean chemical reaction rate $\overline{\dot{\omega}}$ (which has also been verified for the cases considered here). Therefore, according to Equation (3), the mean chemical reaction rate $\overline{\dot{\omega}}$ is usually modeled as:

$$\overline{\dot{\omega}} \approx \overline{(\rho S_d)}_s \Sigma_{gen} \tag{21}$$

For the unity Lewis number cases, $\overline{(\rho S_d)}_s$ is often modeled as $\rho_o S_L$ (Boger et al. 1998; Hawkes and Cant 2000; Hernández-Pérez et al. 2011; Reddy and Abraham 2012). The expressions for the different reaction rate models are shown in Table 1. The variations of $\rho_o S_L \Sigma_{gen}$ (Model 1) are also shown in Figure 12, which indicates that $\rho_o S_L \Sigma_{gen}$ satisfactorily captures the behaviour of $\overline{\dot{\omega}}$ obtained from DNS data when the flame is away from the wall in both cases. However, $\rho_o S_L \Sigma_{gen}$ (Model 1) overpredicts $\overline{\dot{\omega}}$ in the near wall region during FWI for both cases considered here. This overprediction is a consequence of the non-zero value of $\Sigma_{gen} = \overline{|\quad c|}$ at the wall, whereas $\overline{\dot{\omega}}$ vanishes in the near wall region during the flame quenching. This behaviour is also in line with the previous studies (Katragadda, Malkeson, and Chakraborty 2011; Sellmann et al. 2017). Bruneaux, Poinsot, and Ferziger (1997)

**Table 1.** Different reaction rate models.

| | Reaction rate Model |
|---|---|
| Model 1 | $\overline{\dot{\omega}} = \rho_o S_L \Sigma_{gen}$ |
| Model 2 | $\overline{\dot{\omega}} = Q_m \rho_o S_L \Sigma_{gen}$ |
| Model 3 | $\overline{\dot{\omega}} = \rho_o S_{L\ gen}\left(1 + c_y \tilde{A}_w\right) \times \exp\left[-\beta\left\{\left(\tau\tilde{A}\right)/\left(1 + \tau\tilde{\theta}\right)(1 + \tau\tilde{c})\right\}^{c_x}\right]$, where $c_x = 0.25$ and $c_y = 48.0$ represents the model parameters, and $\tilde{A} = \left(\tilde{c} - \tilde{\theta}\right)$ is a non-adiabaticity parameter |
| Model 4 | $\overline{\dot{\omega}} = A_7(\rho_o S_L)\Sigma_{gen}$, where $A_7 = 0.5[\mathrm{erf}(y/\delta_Z - 0.7Pe_{min}) + 1]$ |

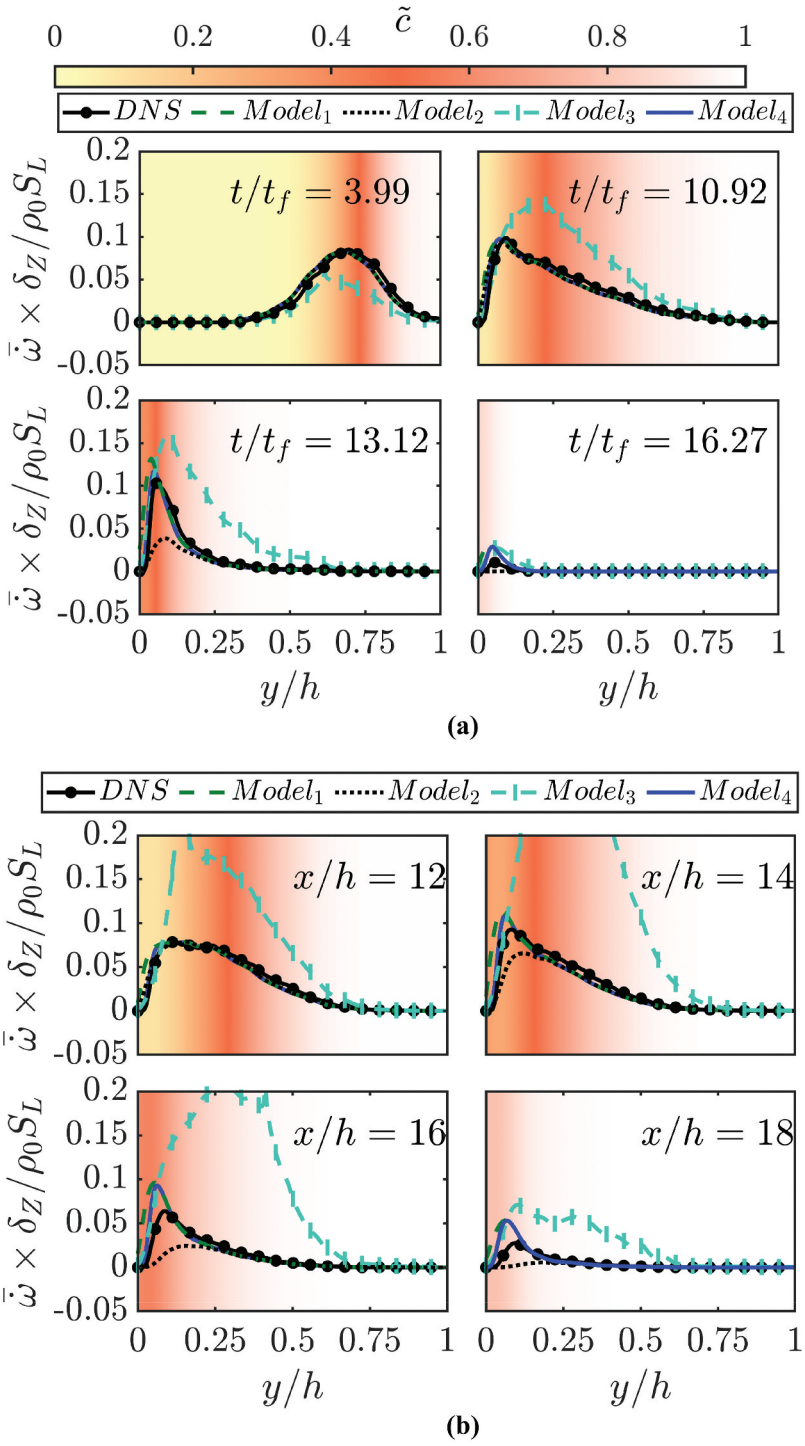


**Figure 12.** Variations of $\overline{\dot{\omega}} \times \delta_Z/\rho_0 S_L$ with $y/h$ as obtained from DNS (black symbols) and predictions of $\rho_0 S_L \Sigma_{gen}$ (Model 1), $Q_m \rho_o S_L \Sigma_{gen}$ (Model 2), $\rho_0 S_{L\ gen}\left(1 + c_y \tilde{A}_w\right) \times \exp\left[-\beta\left\{(\tau\tilde{A})/\left[\left(1 + \tau\tilde{\theta}\right)(1 + \tau\tilde{c})\right]\right\}^{c_x}\right]$ (Model 3), $A_7(\rho_o S_L)\Sigma_{gen}$ with $A_7 = 0.5[\mathrm{erf}(y/\delta_Z - 0.7Pe_{min}) + 1]$ (Model 4), and $A_7(\rho_o S_L)\Sigma_{gen}$ with $A_7 = 0.5[\mathrm{erf}(y/\delta_Z - Pe_{min}) + 1]$ (Model 5) for the (a) unsteady HOI and (b) statistically stationary V-flame OWI cases.

implemented a modification to incorporate the near wall behaviour to the conventional closure model of mean chemical reaction rate $\overline{\dot{\omega}}$ and proposed a damping factor $Q_m = \exp\left[-2\beta\left(\tilde{c}-\tilde{\theta}\right)\right]$ in the model expression for the mean chemical reaction rate $\overline{\dot{\omega}}$ $=Q_m\rho_o S_L\Sigma_{gen}$ (Model 2) so that the parameter $Q_m$ is unity when the flame is away from the wall where $\overline{\dot{\omega}}=\rho_o S_L\Sigma_{gen}$ is recovered, and a small value of $Q_m$ is obtained in the near-wall region, which dampens the magnitude of $Q_m\rho_o S_L\Sigma_{gen}$. The prediction of $\overline{\dot{\omega}}=Q_m\rho_o S_L\Sigma_{gen}$ (Model 2) is also shown in Figure 12, which indicates that the predictions of $Q_m\rho_o S_L\Sigma_{gen}$ are similar to that of $\rho_o S_L\Sigma_{gen}$when the flame is away from the wall but $Q_m\rho_o S_L\Sigma_{gen}$ underpredicts $\overline{\dot{\omega}}$ close to the wall before the flame is quenched.

Alshaalan and Rutland (1998) also suggested the near-wall modification to the conventional closure model of $\overline{\dot{\omega}}$. The predictions from Alshaalan and Rutland (1998) significantly underpredict the values of the mean chemical reaction rate (i.e., $\overline{\dot{\omega}} = \rho_o S_L\ {}_{gen}\left(1+c_y\tilde{A}_w\right)\times\exp\left[-\beta\{\left(\tau\tilde{A}\right)/[\left(1+\tau\tilde{\theta}\right)(1+\tau\tilde{c})]\}^{c_x}\right]$ where $c_x = 0.25$ and $c_y = 48$ are the model parameters, $\tilde{A} = \left(\tilde{c}-\tilde{\theta}\right)$ is a non-adiabaticity parameter) when the flame is away from the wall for the HOI case as shown in Sellmann et al. (2017). It can be seen from Figure 12 that $\overline{\dot{\omega}} = \rho_o S_L\ {}_{gen}\left(1+c_y\tilde{A}_w\right)\backslash\text{break}\times\exp\left[-\beta\{\left(\tau\tilde{A}\right)/[\left(1+\tau\tilde{\theta}\right)(1+\tau\tilde{c})]\}^{c_x}\right]$ (Model 3) significantly overpredicts the mean chemical reaction rate when the flame is away from the wall. However, in the near wall region the predictions of Model 3 are reasonably accurate. More recently, Sellmann et al. (2017) proposed a near-wall modification to the conventional mean chemical reaction rate $\overline{\dot{\omega}}$ $=A_7\left(\rho_o S_L\right)\Sigma_{gen}$ (Model 4), where $A_7 = 0.5[\text{erf}(y/\delta_Z - 0.7Pe_{min})+1]$ is a wall correction which damps the magnitude of the mean chemical reaction rate in the near wall region $y/\delta_Z \ll Pe_{min}$ and asymptotically approaches unity for $y/\delta_Z \gg Pe_{min}$. In Figure 12, it is evident that Model 4 adeptly captures the wall-normal variations of $\overline{\dot{\omega}}$ for both cases considered here at all stages of FWI. Overall, the predictions of Model 4 are in better agreement with DNS data than the other models. However, there is a slight overprediction in the peak values of the $\overline{\dot{\omega}}$ during the advanced stages of the flame quenching. Therefore, Model 4 can be employed for the mean chemical reaction rate closure during FWI within turbulent boundary layers provided the FSD $\Sigma_{gen}$ is satisfactorily modeled.

## Conclusions

The statistical behavior of generalised FSD and its transport equation during FWI within turbulent boundary layers in the context of RANS has been analysed using three-dimensional DNS databases corresponding to a friction Reynolds number of $Re_\tau = 110$. One of these databases pertains to the unsteady HOI of a statistical planar flame propagating into a fully developed turbulent boundary layer, while the other database focuses on the statistically stationary OWI of a turbulent premixed V-flame in a channel flow interacting with inert isothermal channel walls. The findings demonstrate that the presence of the wall has a significant influence on the statistical behaviors of the unclosed terms in the FSD transport equation and the FSD-based mean chemical reaction rate closure. In both cases analysed in this work, the tangential strain rate term assumes positive values throughout the flame

brush, serving as a leading order source term. By contrast, the curvature term acts as the leading order sink term in the FSD transport equation. The relative magnitudes of different terms change from one configuration to another and also with the progress of FWI. This suggests that the orientation of the flame normal vector in relation to the wall normal vector plays a crucial role in the statistical behavior and modelling of the FSD transport equation. This is reflected in the modelling of the unresolved dilatation and unresolved normal strain rate contributions to the tangential strain rate term in the FSD transport equation. It has been observed that the existing models for the tangential strain rate term in the FSD transport equation, which were originally proposed for flames without walls, are insufficient to capture the behavior obtained from DNS data. Therefore, new models for the dilatation and normal strain rate contributions to the tangential strain rate term have been proposed to incorporate the effects of flame orientation, local alignment of the reactive scalar gradient with strain rate eigenvectors and decoupling of nondimensional temperature and reaction progress variable during FWI within turbulent boundary layers. The newly proposed models for the dilatation rate and normal strain rate contributions of the tangential strain rate term have been demonstrated to yield satisfactory qualitative and quantitative agreement with the corresponding terms extracted from DNS data. The previously proposed model expressions for the unclosed turbulent flux of FSD and the combined contributions of the FSD curvature and propagation terms have been revised based on a priori DNS analysis so that they remain valid during FWI within turbulent boundary layers for both HOI and OWI configurations. The revised model expressions have been demonstrated to yield reliable predictions of the relevant terms obtained from DNS data. The conventional closures of mean chemical reaction rate based on FSD provides non-zero predictions in the proximity of the wall even when the flame is completely quenched. Therefore, a model expression, which can adequately capture the drop in the mean chemical reaction rate in the vicinity of the wall due to flame quenching, has been identified and its satisfactory performance has been demonstrated by comparing its prediction with the mean chemical reaction rate obtained from DNS data. Therefore, the proposed model expression can be used to close the mean chemical reaction rate in the presence of FWI occurring within turbulent boundary layers across various flow configurations, provided the FSD $_{gen}$ is satisfactorily modeled. The newly proposed model expressions of the unclosed terms in the FSD transport equation are not expected to increase the computational time significantly in comparison to the conventional models but a slight increase in computational time (i.e., at most by 1–2%) is expected due to the usage of exponential terms and error functions in model parameters.

While previous analyses (Lai et al. 2022; Lai, Klein, and Chakraborty 2018) have documented satisfactory qualitative and quantitative agreement for the FSD and reaction rate closures based on FSD between simplified and detailed chemistry DNS results, it remains essential to validate the statistical observations presented in this paper, considering the impact of detailed chemistry and transport, especially at higher Reynolds numbers.

## Disclosure statement

There are no pertinent competing interests for the authors to declare concerning the content of this article.

## Funding

The authors extend their appreciation for the financial and computational assistance provided by the Engineering and Physical Sciences Research Council (Grant: EP/V003534/1 and EP/R029369/1), along with support from CIRRUS and ROCKET (Newcastle University's HPC facility).

## Author contribution

NC conceived the analysis, and NC and SKG authored the initial version of the paper. UA and SKG conducted the simulations, with SKG creating the figures. NC, UA, and SKG contributed to revising the manuscript. NC and UA provided supervision for SKG.

## References

Abu-Orf, G. M., and R. S. Cant. 2000. A turbulent reaction rate model for premixed turbulent combustion in spark-ignition engines. *Combust. Flame* 122 (3):233–252. doi:10.1016/S0010-2180(00)00123-1.

Ahmed, U., D. Apsley, T. Stallard, P. Stansby, and I. Afgan. 2021. Turbulent length scales and budgets of Reynolds stress-transport for open-channel flows; friction Reynolds numbers Re_τ =150, 400 and 1020. *J. Hydraul. Res.* 59 (1):36–50. doi:10.1080/00221686.2020.1729265.

Ahmed, U., N. Chakraborty, and M. Klein. 2021a. Assessment of Bray Moss Libby formulation for premixed flame-wall interaction within turbulent boundary layers: Influence of flow configuration. *Combust. Flame* 233:111575. doi:10.1016/j.combustflame.2021.111575.

Ahmed, U., N. Chakraborty, and M. Klein. 2021b. Influence of thermal wall boundary condition on scalar statistics during flame-wall interaction of premixed combustion in turbulent boundary layers. *Int. J. Heat Fluid Flow* 92:108881. doi:10.1016/j.ijheatfluidflow.2021.108881.

Ahmed, U., N. Chakraborty, and M. Klein. 2021c. Scalar gradient and strain rate statistics in oblique premixed flame-wall interaction within turbulent channel flows. *Flow Turbul. Combust.* 106 (2):701–32. doi:10.1007/s10494-020-00169-3.

Ahmed, U., N. Chakraborty, and M. Klein. 2023. Influence of flow configuration and thermal wall boundary conditions on turbulence during premixed flame-wall interaction within low Reynolds number boundary layers. *Flow Turbul. Combust.* 111 (3):825–66. doi:10.1007/s10494-023-00437-y.

Ahmed, U., A. L. Pillai, N. Chakraborty, and R. Kurose. 2020. Surface density function evolution and the influence of strain rates during turbulent boundary layer flashback of hydrogen-rich premixed combustion. *Phys. Fluids* 32 (5):055112. doi:10.1063/5.0004850.

Alshaalan, T., and C. J. Rutland. 2002. Wall heat flux in turbulent premixed reacting flow. *Combust. Sci. Technol.* 174 (1):135–165. doi:10.1080/713712913.

Alshaalan, T. M., and C. J. Rutland. 1998. Turbulence, scalar transport, and reaction rates in flame-wall interaction. *Twenty-Seventh Symp. (Int.) Combust. Vols. 1 And 2* 27 (1):793–99. doi:10.1016/S0082-0784(98)80474-8.

Balint, J.-L., P. Vukoslavcevic, and J. M. Wallace. 1990. The transport of enstrophy in a turbulent boundary layer. In *Near-wall turbulence*, 932–50. https://ui.adsabs.harvard.edu/abs/1990nrw.book.932B .

Berger, L., A. Attili, and H. Pitsch. 2022. Synergistic interactions of thermodiffusive instabilities and turbulence in lean hydrogen flames. *Combust. Flame* 244:112254. doi:10.1016/j.combustflame.2022.112254.

Boger, M., D. Veynante, H. Boughanem, and A. Trouve. 1998. Direct numerical simulation analysis of flame surface density concept for large eddy simulation of turbulent premixed combustion. *Twenty-Seventh Symp. (Int.) Combust. Vols. 1 And 2* 27 (1):917–25. doi:10.1016/S0082-0784(98)80489-X.

Bray, K. N. C. 1990. Studies of the turbulent burning velocity. *Proc. R. Soc. Lond. A. Math. Phys. Sci.* 431 (1882):315–35.

Bray, K. N. C., P. A. Libby, and J. B. Moss. 1985. Unified modeling approach for premixed turbulent combustion—part I: General formulation. *Combust. Flame* 61 (1):87–102. doi:10.1016/0010-2180(85)90075-6.

Bruneaux, G., K. Akselvoll, T. Poinsot, and J. H. Ferziger. 1996. Flame-wall interaction simulation in a turbulent channel flow. *Combust. Flame* 107 (1–2):27–36. doi:10.1016/0010-2180(95)00263-4.

Bruneaux, G., T. Poinsot, and J. H. Ferziger. 1997. Premixed flame-wall interaction in a turbulent channel flow: Budget for the flame surface density evolution equation and modelling. *J. Fluid Mech.* 349:191–219. doi:10.1017/S0022112097006769.

Candel, S. M., and T. J. Poinsot. 1990. Flame stretch and the balance equation for the flame area. *Combust. Sci. Technol.* 70 (1–3):1–15. doi:10.1080/00102209008951608.

Candel, S., D. P. Veynante, F. Lacas, E. Maistret, N. Darabiha, and T. Poinsot. 1990. Coherent flamelet model: Applications and recent extensions.

Cant, R. S., and K. N. C. Bray. 1989a. Strained laminar flamelet calculations of premixed turbulent combustion in a closed vessel. *Symp. (Int.) Combust.* 22 (1):791–799. doi:10.1016/S0082-0784(89)80088-8.

Cant, R. S., and K. N. C. Bray. 1989b. A theoretical model of premixed turbulent combustion in closed vessels. *Combust. Flame* 76 (3):243–63. doi:10.1016/0010-2180(89)90109-0.

Cant, R. S., S. B. Pope, and K. N. C. Bray. 1991. Modelling of flamelet surface-to-volume ratio in turbulent premixed combustion. *Symp. (Int.) Combust.* 23 (1):809–815. doi:10.1016/S0082-0784(06)80334-6.

Chakraborty, N., and R. S. Cant. 2007. A priori analysis of the curvature and propagation terms of the flame surface density transport equation for large eddy simulation. *Phys. Fluids* 19 (10). doi:10.1063/1.2772326.

Chakraborty, N., and R. S. Cant. 2009a. Direct numerical simulation analysis of the flame surface density transport equation in the context of large eddy simulation. *Proc. Combust. Inst.* 32 (1):1445–53. doi:10.1016/j.proci.2008.06.028.

Chakraborty, N., and R. S. Cant. 2009b. Effects of Lewis number on turbulent scalar transport and its modelling in turbulent premixed flames. *Combust. Flame* 156 (7):1427–1444. doi:10.1016/j.combustflame.2009.03.010.

Chakraborty, N., and R. S. Cant. 2011. Effects of Lewis number on flame surface density transport in turbulent premixed combustion. *Combust. Flame* 158 (9):1768–1787. doi:10.1016/j.combustflame.2011.01.011.

Chakraborty, N., and R. S. Cant. 2013. Turbulent Reynolds number dependence of flame surface density transport in the context of Reynolds averaged navier–stokes simulations. *Proc. Combust. Inst.* 34 (1):1347–56. doi:10.1016/j.proci.2012.07.071.

Chakraborty, N., and M. Klein. 2008. A priori direct numerical simulation assessment of algebraic flame surface density models for turbulent premixed flames in the context of large eddy simulation. *Phys. Fluids* 20 (8). doi:10.1063/1.2969474.

Chakraborty, N., M. Klein, and N. Swaminathan. 2009. Effects of Lewis number on the reactive scalar gradient alignment with local strain rate in turbulent premixed flames. *Proc. Combust. Inst.* 32 (1):1409–17. doi:10.1016/j.proci.2008.06.021.

Chakraborty, N., and N. Swaminathan. 2007. Influence of the Damköhler number on turbulence-scalar interaction in premixed flames. I. Physical insight. *I. Phys. Insight* 19 (4):*Physics of Fluids*, *19* (4. doi:10.1063/1.2714070.

Charlette, F., C. Meneveau, and D. Veynante. 2002. A power-law flame wrinkling model for LES of premixed turbulent combustion part I: Non-dynamic formulation and initial tests. *Combust. Flame* 131 (1):159–80. doi:10.1016/S0010-2180(02)00400-5.

Duclos, J. M., D. Veynante, and T. Poinsot. 1993. A comparison of flamelet models for premixed turbulent combustion. *Combust. Flame* 95 (1):101–17. doi:10.1016/0010-2180(93)90055-8.

Dunstan, T. D., N. Swaminathan, K. N. C. Bray, and R. S. Cant. 2010. Geometrical properties and turbulent flame speed measurements in stationary premixed V-flames using direct numerical simulation. *Flow Turbul. Combust.* 87 (2–3):237–59. doi:10.1007/s10494-010-9284-1.

Fureby, C. 2005. A fractal flame-wrinkling large eddy model for premixed turbulent simulation combustion. *Proc. Combust. Inst.* 30 (1):593–601. doi:10.1016/j.proci.2004.08.068.

Ghai, S. K., U. Ahmed, and N. Chakraborty. 2023a. Effects of fuel Lewis number on wall heat transfer during oblique flame-wall interaction of premixed flames within turbulent boundary layers. *Flow Turbul. Combust.* 111 (3):867–895. doi:10.1007/s10494-023-00418-1.

Ghai, S. K., U. Ahmed, and N. Chakraborty. 2023b. Statistical behaviour and modelling of variances of reaction progress variable and temperature during flame-wall interaction of premixed flames within turbulent boundary layers. *Flow Turbul. Combust*. doi:10.1007/s10494-023-00439-w.

Ghai, S. K., U. Ahmed, N. Chakraborty, and M. Klein. 2022. Entropy generation during head-on interaction of premixed flames with inert walls within turbulent boundary layers. *Entropy* 24 (4):463. doi:10.3390/e24040463.

Ghai, S. K., U. Ahmed, M. Klein, and N. Chakraborty. 2022. Energy integral equation for premixed flame-wall interaction in turbulent boundary layers and its application to turbulent burning velocity and wall flux evaluations. *Int. J. Heat Mass Transfer* 196:123230. doi:10.1016/j.ijheatmasstransfer.2022.123230.

Ghai, S. K., U. Ahmed, M. Klein, and N. Chakraborty. 2023. Turbulent kinetic energy evolution in turbulent boundary layers during head-on interaction of premixed flames with inert walls for different thermal boundary conditions. *Proc. Combust. Inst.* 39 (2):2169–78. doi:10.1016/j.proci.2022.08.055.

Ghai, S. K., N. Chakraborty, U. Ahmed, and M. Klein. 2022. Enstrophy evolution during head-on wall interaction of premixed flames within turbulent boundary layers. *Phys. Fluids* 34 (7):075124. doi:10.1063/5.0098047.

Gorski, J. J., J. M. Wallace, and P. S. Bernard. 1994. The enstrophy equation budget of bounded turbulent shear flows. *Phys. Fluids* 6 (9):3197–3199. doi:10.1063/1.868100.

Gruber, A., R. Sankaran, E. R. Hawkes, and J. H. Chen. 2010. Turbulent flame-wall interaction: A direct numerical simulation study. *J. Fluid Mech.* 658:5–32. doi:10.1017/S0022112010001278.

Gupta, S. K., R. Palulli, M. Talei, R. L. Gordon, and V. K. Arghode. 2022. CO modelling of premixed head-on quenching flame in the context of large-eddy simulation. *Int. J. Heat Fluid Flow* 93:108895. doi:10.1016/j.ijheatfluidflow.2021.108895.

Han, I., and K. Y. Huh. 2008. Roles of displacement speed on evolution of flame surface density for different turbulent intensities and Lewis numbers in turbulent premixed combustion. *Combust. Flame* 152 (1):194–205. doi:10.1016/j.combustflame.2007.10.003.

Hawkes, E. R., and R. S. Cant. 2000. A flame surface density approach to large-eddy simulation of premixed turbulent combustion. *Proc. Combust. Inst.* 28 (1):51–58. doi:10.1016/S0082-0784(00)80194-0.

Hawkes, E. R., and R. S. Cant. 2001. Implications of a flame surface density approach to large eddy simulation of premixed turbulent combustion. *Combust. Flame* 126 (3):1617–1629. doi:10.1016/S0010-2180(01)00273-5.

Hernández-Pérez, F. E., F. T. C. Yuen, C. P. T. Groth, and Ö. L. Gülder. 2011. LES of a laboratory-scale turbulent premixed bunsen flame using FSD, PCM-FPI and thickened flame models. *Proc. Combust. Inst.* 33 (1):1365–71. doi:10.1016/j.proci.2010.06.010.

Jainski, C., M. Rissmann, B. Bohm, and A. Dreizler. 2017. Experimental investigation of flame surface density and mean reaction rate during flame-wall interaction. *Proc. Combust. Inst.* 36 (2):1827–34. doi:10.1016/j.proci.2016.07.113.

Jainski, C., M. Rissmann, B. Bohm, J. Janicka, and A. Dreizler. 2017. Sidewall quenching of atmospheric laminar premixed flames studied by laser-based diagnostics. *Combust. Flame* 183:271–282. doi:10.1016/j.combustflame.2017.05.020.

Jainski, C., M. Rissmann, S. Jakirlic, B. Bohm, and A. Dreizler. 2018. Quenching of premixed flames at cold walls: Effects on the local flow field. *Flow Turbul. Combust.* 100 (1):177–196. doi:10.1007/s10494-017-9836-8.

Jenkins, K. W., and R. S. Cant. 1999. Direct numerical simulation of turbulent flame kernels. In *Recent advances in DNS and LES*, ed. D. Knight and L. Sakell, 191–202. Dordrecht: Springer, Netherlands.

Katragadda, M., Y. Gao, and N. Chakraborty. 2014. Modeling of the strain rate contribution to the flame surface density transport for non-unity Lewis number flames in large eddy simulations. *Combust. Sci. Technol.* 186 (10–11):1338–1369. doi:10.1080/00102202.2014.934584.

Katragadda, M., S. P. Malkeson, and N. Chakraborty. 2011. Modelling of the tangential strain rate term of the flame surface density transport equation in the context of Reynolds averaged Navier-stokes simulation. *Proc. Combust. Inst.* 33 (1):1429–37. doi:10.1016/j.proci.2010.06.129.

Katragadda, M., S. P. Malkeson, and N. Chakraborty. 2014. Modelling of the curvature term in the flame surface density transport equation: A direct numerical simulations based analysis. *Int. J. Spray Combust. Dyn.* 6 (2):163–198. doi:10.1260/1756-8277.6.2.163.

Keil, F. B., M. Amzehnhoff, U. Ahmed, N. Chakraborty, and M. Klein. 2021a. Comparison of flame propagation statistics based on direct numerical simulation of simple and detailed chemistry. Part 2: Influence of choice of reaction progress variable. *Energies* 14 (18):5695. doi:10.3390/en14185695.

Keil, F. B., M. Amzehnhoff, U. Ahmed, N. Chakraborty, and M. Klein. 2021b. Comparison of flame propagation statistics extracted from direct numerical simulation based on simple and detailed chemistry—part 1: Fundamental flame turbulence interaction. *Energies* 14 (17):5548. doi:10.3390/en14175548.

Keil, F. B., N. Chakraborty, and M. Klein. 2020. Flame surface density transport statistics for high pressure turbulent premixed bunsen flames in the context of large eddy simulation. *Combust. Sci. Technol.* 192 (11):2070–2092. doi:10.1080/00102202.2020.1789122.

Keppeler, R., E. Tangermann, U. Allaudin, and M. Pfitzner. 2014. LES of low to high turbulent combustion in an elevated pressure environment. *Flow Turbul. Combust.* 92 (3):767–802. doi:10.1007/s10494-013-9525-1.

Klein, M., N. Chakraborty, and M. Pfitzner. 2016. Analysis of the combined modelling of sub-grid transport and filtered flame propagation for premixed turbulent combustion. *Flow Turbul. Combust.* 96 (4):921–938. doi:10.1007/s10494-016-9714-9.

Knikker, R., D. Veynante, and C. Meneveau. 2002. A priori testing of a similarity model for large eddy simulations of turbulent premixed combustion. *Proc. Combust. Inst.* 29 (2):2105–11. doi:10.1016/S1540-7489(02)80256-5.

Lai, J., U. Ahmed, M. Klein, and N. Chakraborty. 2022. A comparison between head-on quenching of stoichiometric methane-air and hydrogen-air premixed flames using direct numerical simulations. *Int. J. Heat Fluid Flow* 93:108896. doi:10.1016/j.ijheatfluidflow.2021.108896.

Lai, J. W., and N. Chakraborty. 2016. Modeling of progress variable variance transport in head-on quenching of turbulent premixed flames: A direct numerical simulation analysis. *Combust. Sci. Technol.* 188 (11–12):1925–1950. doi:10.1080/00102202.2016.1211868.

Lai, J., M. Klein, and N. Chakraborty. 2017. Assessment of algebraic flame surface density closures in the context of large eddy simulations of head-on quenching of turbulent premixed flames. *Combust. Sci. Technol.* 189 (11):1966–1991. doi:10.1080/00102202.2017.1347161.

Lai, J., M. Klein, and N. Chakraborty. 2018. Direct numerical simulation of head-on quenching of statistically planar turbulent premixed methane-air flames using a detailed chemical mechanism. *Flow Turbul. Combust.* 101 (4):1073–1091. doi:10.1007/s10494-018-9907-5.

Lai, J., A. Moody, and N. Chakraborty. 2017. Turbulent kinetic energy transport in head-on quenching of turbulent premixed flames in the context of Reynolds averaged navier stokes simulations. *Fuel* 199:456–477. doi:10.1016/j.fuel.2017.02.091.

Lai, J., D. H. Wacks, and N. Chakraborty. 2018. Flow topology distribution in head-on quenching of turbulent premixed flame: A direct numerical simulation analysis. *Fuel* 224:186–209. doi:10.1016/j.fuel.2018.03.021.

Luca, S., A. Attili, E. Lo Schiavo, F. Creta, and F. Bisetti. 2019. On the statistics of flame stretch in turbulent premixed jet flames in the thin reaction zone regime at varying Reynolds number. *Proc. Combust. Inst.* 37 (2):2451–59. doi:10.1016/j.proci.2018.06.194.

Ma, T., O. T. Stein, N. Chakraborty, and A. M. Kempf. 2013. A posteriori testing of algebraic flame surface density models for LES. *Combust. Theor. Model.* 17 (3):431–482. doi:10.1080/13647830.2013.779388.

Ma, T., O. T. Stein, N. Chakraborty, and A. M. Kempf. 2014. A posteriori testing of the flame surface density transport equation for LES. *Combust. Theor. Model.* 18 (1):32–64. doi:10.1080/13647830.2013.848383.

Moser, R. D., J. Kim, and N. N. Mansour. 1999. Direct numerical simulation of turbulent channel flow up to Reτ=590. *Phys. Fluids* 11 (4):943–945. doi:10.1063/1.869966.

Papapostolou, V., N. Chakraborty, M. Klein, and H. G. Im. 2019. Effects of reaction progress variable definition on the flame surface density transport statistics and closure for different combustion regimes. *Combust. Sci. Technol.* 191 (8):1276–1293. doi:10.1080/00102202.2018.1523152.

Peters, N. 2000. *Turbulent Combustion*. Ist ed. Cambridge, UK: Cambridge University Press.

Poinsot, T. J., D. C. Haworth, and G. Bruneaux. 1993. Direct simulation and modeling of flame-wall interaction for premixed turbulent combustion. *Combust. Flame* 95 (1–2):118–132. doi:10.1016/0010-2180(93)90056-9.

Pope, S. B. 1988. The evolution of surfaces in turbulence. *Int. J. Eng. Sci.* 26 (5):445–469. doi:10.1016/0020-7225(88)90004-3.

Rasool, R., M. Klein, and N. Chakraborty. 2022. Flame surface density based mean reaction rate closure for Reynolds averaged Navier Stokes methodology in turbulent premixed bunsen flames with non-unity Lewis number. *Combust. Flame* 239:111766. doi:10.1016/j.combustflame.2021.111766.

Reddy, H., and J. Abraham. 2012. Two-dimensional direct numerical simulation evaluation of the flame-surface density model for flames developing from an ignition kernel in lean methane/air mixtures under engine conditions. *Phys. Fluids* 24 (10). doi:10.1063/1.4757655.

Sellmann, J., J. W. Lai, A. M. Kempf, and N. Chakraborty. 2017. Flame surface density based modelling of head-on quenching of turbulent premixed flames. *Proc. Combust. Inst.* 36 (2):1817–25. doi:10.1016/j.proci.2016.07.114.

Trouvé, A., and T. Poinsot. 1994. The evolution equation for the flame surface density in turbulent premixed combustion. *J. Fluid Mech.* 278:1–31. doi:10.1017/S0022112094003599.

Varma, A. R., U. Ahmed, and N. Chakraborty. 2021. Effects of body forces on the statistics of flame surface density and its evolution in statistically planar turbulent premixed flames. *Flow Turbul. Combust.* 108 (1):181–212. doi:10.1007/s10494-021-00268-9.

Varma, A. R., U. Ahmed, and N. Chakraborty. 2023. Turbulence effects on the statistical behaviour and modelling of flame surface density and the terms of its transport equation in turbulent premixed flames. *Flow Turbul. Combust.* 111 (2):531–565. doi:10.1007/s10494-023-00430-5.

Veynante, D., J. Piana, J. M. Duclos, and C. Martel. 1996. Experimental analysis of flame surface density models for premixed turbulent combustion. *Symp. (Int.) Combust.* 26 (1):413–420. doi:10.1016/S0082-0784(96)80243-8.

Veynante, D., A. Trouve, K. N. C. Bray, and T. Mantel. 1997. Gradient and counter-gradient scalar transport in turbulent premixed flames. *J. Fluid Mech.* 332:263–293. doi:10.1017/S0022112096004065.

Watkins, A. P., S. P. Li, and R. S. Cant (1996). Premixed combustion modelling for spark-ignition engine applications. *SAE Technical Paper* 961190

Yoo, C. S., and H. G. Im. 2007. Characteristic boundary conditions for simulations of compressible reacting flows with multi-dimensional, viscous and reaction effects. *Combust. Theor. Model.* 11 (2):259–286. doi:10.1080/13647830600898995.

Zhao, P. P., L. P. Wang, and N. Chakraborty. 2018. Analysis of the flame-wall interaction in premixed turbulent combustion. *J. Fluid Mech.* 848:193–218. doi:10.1017/jfm.2018.356.

Zhao, D., C. Zhang, F. E. Hernández Pérez, H. G. Im, and L. Wang. 2023. Turbulent premixed hydrogen/air flame-wall interaction with heterogeneous surface reactions. *Proc. Combust. Inst.* 39 (2):2189–97. doi:10.1016/j.proci.2022.09.018.